STRATEGIES FOR DETECTING POOR COUPLING

IN AN OBS EXPERIMENT

A Thesis

by

FITRIX PRIMANTORO PUTRO

Submitted to the Office of Graduate Studies of
Texas A&M University
in partial fulfillment of the requirements for the degree of

MASTER OF SCIENCE

August 2003

Major Subject: Geophysics

STRATEGIES FOR DETECTING POOR COUPLING

IN AN OBS EXPERIMENT

A Thesis

by

FITRIX PRIMANTORO PUTRO

Submitted to Texas A&M University
in partial fulfillment of the requirements
for the degree of

MASTER OF SCIENCE

Approved as to style and content by:

Luc T. Ikelle (Chair of Committee)	Joel S. Watkins (Member)
Walter B. Ayers, Jr (Member)	Andrew Hajash, Jr (Head of Department)

August 2003

Major Subject: Geophysics

ABSTRACT

Strategies for Detecting Poor Coupling

in an OBS Experiment. (August 2003)

Fitrix Primantoro Putro, B.S., Institute of Technology of Bandung

Chair of Advisory Committee: Dr. Luc T. Ikelle

We present a method for detecting and correcting poor coupling in an Ocean Bottom Seismic (OBS) experiment. The basic idea of our method is that the normal component (with respect to the seafloor) of particle velocity is continuous at the water-solid interface. A comparison of the normal component of particle velocity just above and below the seafloor allows us to assess poor coupling. In other words, our method for detecting poor coupling consists of analyzing vertical particle velocities measured just above and below the seafloor. The normal component of particle velocity above the water is measured using either a vertical receiver array or a vertical source array (dipole source), whereas the normal component of particle velocity below the water is directly measured in this OBS experiment.

In general, the quantities recorded in the OBS experiment are vertical and horizontal components of particle velocity, but continuity of the boundary is based on the normal component of particle velocity being oriented perpendicularly to the seafloor. For a flat seafloor, the vertical component of particle velocity values just above and below the seafloor must be almost equal according to the continuity condition at the

water-solid boundary. However, for a dipping seafloor this is not the case. We have established that we can differentiate a poor coupling effect from a dipping-seafloor effect by using the vertical component of particle velocity.

We have tested our method on real (Eugene Island) data and synthetic (finite-difference) data. For finite-difference synthetics, we have used a grid spacing 0.25 meters to properly simulate the water-solid interface. By examining the uniformity (with respect to offset) of cross-correlation between the vertical component of particle velocity just above and below the seafloor, we were able to detect poor coupling and to differentiate it with any dipping effect at the seafloor. The energy of data just above and below the seafloor were also used for detecting poor coupling and for differentiating it from dipping-seafloor effect.

DEDICATION

Dedicated with love and gratitude to my beloved parents,

Imam Koironi and Siti Muslichah,

whose support for, and confidence in me has provided the impetus for this work.

I could not have gotten to this place without you.

ACKNOWLEDGEMENTS

I would like to especially thank my committee chairman, Dr. Luc T. Ikelle for his guidance, support, and encouragement during the preparation of my thesis.

I appreciate Dr. Joel S. Watkins and Dr. Walter B. Ayers for their suggestions and for their service as members of my graduate advisory committee.

I greatly appreciate the individual efforts of Dr. Kush Tandon for his invaluable collaboration throughout this research.

I am very grateful to all my friends and CASP members for their help and advice during my attendance at this university.

Thanks are also needed to Nick Moldoveanu and Schlumberger who provided me Eugene Island 4C data, as well as all the sponsors of the CASP project that made this and other research possible.

Moreover, I wish to acknowledge the Pertamina-China National Offshore Oil Corporation Consortium for providing me with the scholarship for this study.

Above all, I thank my God for this and many other blessings I am continually and gracefully showered with.

TABLE OF CONTENTS

CHAPTER Page

TABLE OF FIGURES

FIGURE Page

FIGURE Page

FIGURE Page

CHAPTER I

INTRODUCTION

An Ocean Bottom System (OBS) typically consists from 3 geophones (one vertical geophone and two horizontal geophones (X, Y, and Z) and one hydrophone (H_1) as described by Figure 1. Another hydrophone (H_2) could be added to the system in such a way that the two hydrophones could form a vertical hydrophone array (Figure 1). The vertical hydrophone array is connected to the recording system (RS). A small float is connected to the vertical hydrophone array in order to keep the vertical array in a vertical position. The vertical hydrophone array could be used to derive vertical particle velocity (V_z) and also to do wavefield separation of upgoing wavefields and downgoing wavefields. The V_z derived from the vertical hydrophone array could be used to calibrate the coupling of the vertical geophone.

Four components (4C) OBS experiment relied heavily on the accuracy of coupling of geophone at the seafloor. This acquisition system assumes that geophones are physically attached to the seafloor. Otherwise, we end up with biased recordings of particle velocity. Such a biased recording is characterized as poor coupling. In some cases, geophone might end up acting as hydrophone (Figure 2). It is therefore important to develop method for detecting and correcting for any potential coupling of geophone at the seafloor. We here disclose a new method for this purpose. The method is the base on

---

This thesis follows the style and format of Geophysics.

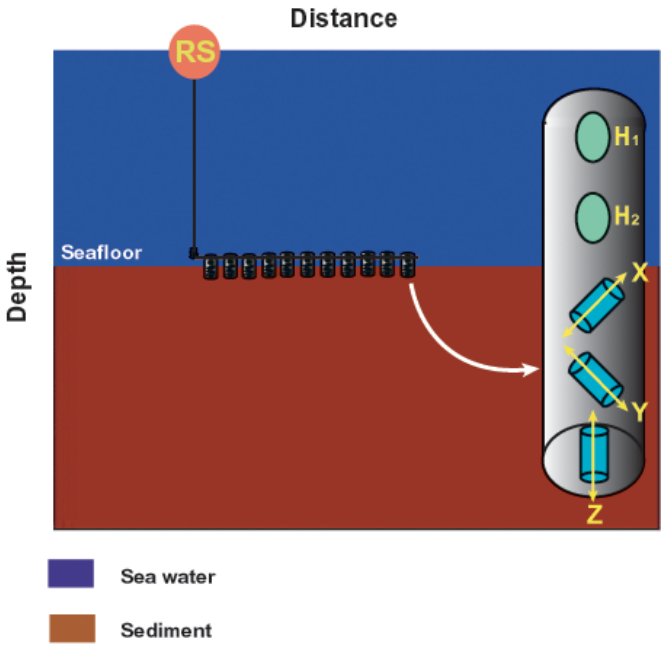

FIG. 1. OBS 4C sensor consists of one hydrophone (H_1) and three orthogonally oriented geophones (X, Y, and Z) to record both pressure and particle velocity. Another hydrophone (H_2) could be added to the system which form a vertical hydrophone array.

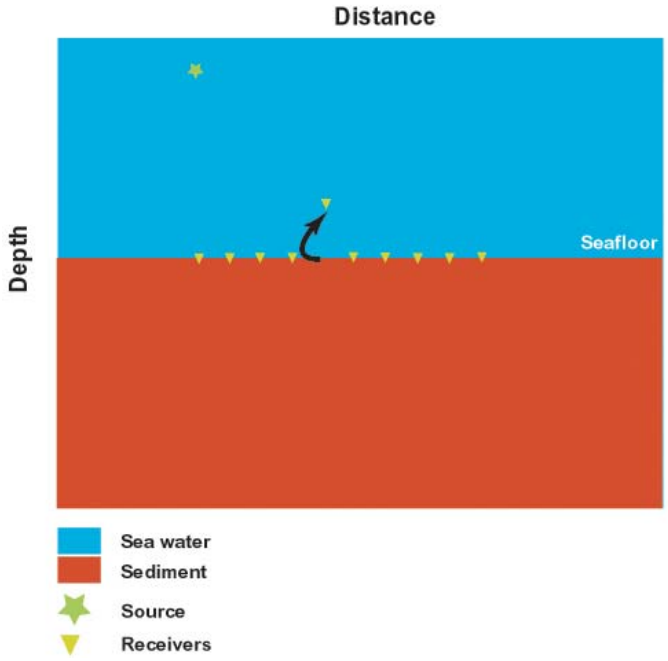

FIG. 2. Poor coupling problem in OBS experiment. Poorly coupled geophone is acting like hydrophone.

the idea that the normal component (with respect to seafloor) of the particle velocity (V_n) is continuous across the seafloor. In the presence of poor coupling, this properties is obviously not valid. The key requirement of this method is that the measurements of the normal component of the particle velocity above and below the seafloor are available. The traditional 4C OBS set up provide such measurement below the seafloor, especially if the seafloor is flat. By using a vertical array of hydrophone in the water or alternatively by using vertical array of monopole sources (dipole) in the water, we can also infer the particle velocity in the water.

Even in the presence of dipping seafloor, traditional OBS acquisition generally record the vertical component of the particle velocity (V_z), instead of the normal component of the particle velocity (V_n) with respect to seafloor. As V_z is not continuous across a dipping seafloor, anomalies in V_z can be due either to poor coupling or dipping effects. Fortunately, the characters of these two effects are so different that so they can be easily separated.

In summary, the objective is to develop a new method for detecting poor coupling. This method can be used during real time acquisition. To avoid potential difficulties related to the measurement and computation of V_z in the water, we have also investigated the possibility of detecting coupling by comparing pressure (P) in the water with V_z below the water.

Notice also, that this method can also detect any potential and perfection of the water-solid interface (seafloor). As such imperfection can appear in a recording in the form of poor coupling.

SCOPE OF THIS THESIS

Strategy for detecting poor coupling in OBS

We will approach the objectives outlined above, initially by introducing some background theories related to the method we have used. More precisely, we will be developing some theoretical background regarding the following issues:

- boundary conditions at a water-solid interface.
- reciprocity theorem for pressure and particle velocity measurements.
- measurement of particle velocity in water (vertical gradient of pressure).
- the use of normalized cross-correlation to measure similarities between measurements just above and below the water-solid interface.
- the use of seismic amplitude to measure similarities between measurements just above and below the water-solid interface.

Detecting poor coupling on synthetic FDM data

Here, synthetic model is generated for some geological models using an elastic finite-difference modeling technique. More precisely, finite-difference modeling software that we used is based on the 2D full elastic wave equations. We will focus on the following issues regarding our usage of this software:

- modeling of water-solid interface; particularly in how small we need the grid space to be for typical seismic frequencies.
- validating the detecting of poor coupling in synthetic data.

- again, using synthetic data to show that the effect of seafloor topography is quite different for poor coupling anomalies.

Preliminary real data test on Eugene Island 4C data

The long term objective of this study is to develop real time diagnostic tools for detecting poor coupling. In other words, we would like to develop a fast and accurate technique which can be used during the acquisition process. In this chapter, we provide a preliminary analysis of Eugene Island 4C survey data.

CHAPTER II

STRATEGY FOR DETECTING POOR COUPLING IN OBS

The basic idea here that when two independent measurements of the particle are available, one measurements just above the seafloor and the other just below the seafloor, we can use the requirements on the boundary conditions at the seafloor to detect any potential poor coupling of geophones.

Before we valid this idea with numerical example, there are two fundamentals aspects that we have to address. The first one is to reiterate the boundary conditions at the seafloor. The second one is to describe how we can infer the measurements of particle velocity above the seafloor. Let us start by the boundary condition.

THEORETICAL BACKGROUND ON WATER-SOLID BOUNDARY CONDITIONS

Consider the interface between a fluid and an elastic medium (Figure 3). We assume that the fluid is non-viscous. At such an interface, slip is allowed in the transverse direction so that only the normal component of the particle velocity vector is constrained by a contact condition. The continuity of V_n reads

$$V_n(x^-) = V_n(x^+)\,, \tag{1}$$

$$\{\ V_n^{(a)} = V_n(x^-)\,;\ \ V_n^{(b)} = V_n(x^+)\ \}$$

where x^- and x^+ denote locations in the fluid and the elastic medium at the interface, respectively (Figure 3). Notice that when the fluid-solid interface is horizontally flat (Figure 4), then V_n is the vertical component of the particle velocity V_z. So for a horizontally flat, the following relation,

$$V_z(z^-) = V_z(z^+)\,, \tag{2}$$

$$\{\ V_z^{(a)} = V_z(z^-)\,;\ \ V_z^{(b)} = V_z(z^+)\ \}$$

where z^- and z^+ denote depths in the fluid and the elastic medium at the interface, respectively.

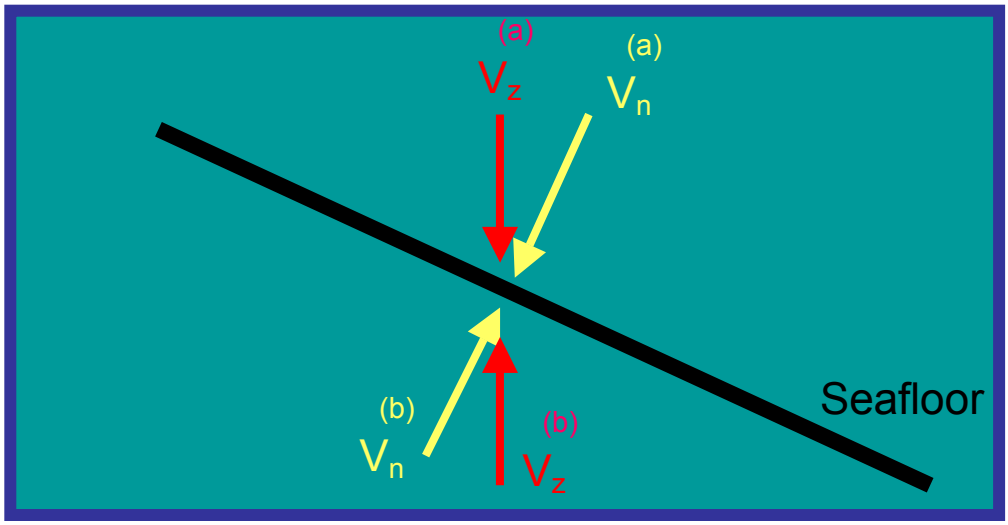

FIG. 3. Boundary across dipping interface.

The equation (1) and (2) are obviously not valid for if the measurements of $V_n(x^+)$ or $V_z(z^+)$ are erroneous as it the case poorly coupled geophone. In other words, for in the presence of poor coupling,

$$V_n\left(x^+\right) \neq V_n\left(x^-\right); \qquad V_z\left(z^+\right) \neq V_z\left(z^-\right). \tag{3}$$

Note also due to the allowed slip in the transverse direction, the transverse components of motion in the elastic medium in general are unrelated to the transverse components of fluid motion:

$$V_{tx}\left(x^+\right) \neq V_{tx}\left(x^-\right); \qquad V_{ty}\left(x^+\right) \neq V_{ty}\left(x^-\right). \tag{4}$$

Thus, for a dipping seafloor, the vertical component of the particle velocity in the solid, which is a combination of V_n, V_{tx}, and V_{ty} are unrelated to that of the fluid:

$$V_z(z^+) \neq V_z(z^-). \tag{5}$$

So our criteria of poor coupling in equation (5) is similar to that of detecting seafloor dipping effect for V_z. We see latter that despite this similarity, the poor coupling can be detected using V_z even for dipping seafloor.

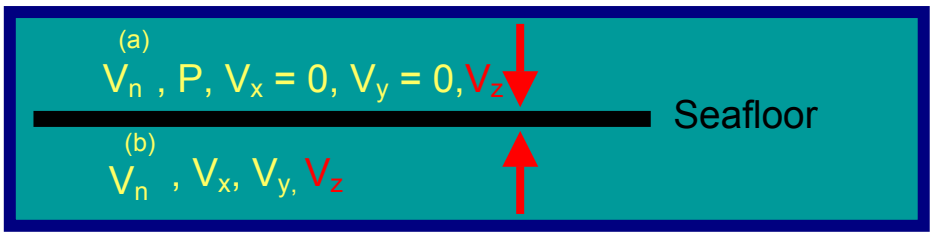

FIG. 4. Boundary across flat interface.

DETERMINATION OF V_z IN THE WATER

As described above, our method of detecting poor coupling require the vertical component of particle velocity, or equivalently, the vertical pressure gradient above and below the seafloor. The vertical component of particle velocity below the seafloor is routinely recorded in OBS surveys. However, the vertical components of particle velocity above the seafloor are not readily available with the current OBS acquisition. The vertical particle velocity can be computed as the vertical gradient of the pressure in x-t domain as follows

$$\frac{\partial v_z}{\partial t} = -\frac{1}{\rho}\frac{\partial p}{\partial z}. \tag{6}$$

where ρ is the density of the water, v_z is the particle velocity data and p is the pressure data expressed as receiver gathers.

Then, how can we obtain the required vertical pressure gradient? Obviously, the best solution, if feasible, is to develop technology to record this data component. Unfortunately, this is not directly possible in water; we have to turn to indirect measurements of the vertical component of the particle velocity in water. We here described two approaches for these indirect measurements.

One alternative technique to obtain the vertical pressure gradient is to introduce data recording with dual hydrophones (i.e. a vertical array of hydrophones) where the pressure field is recorded on hydrophones at two different depth levels (Figure 5). To avoid complex towing a vertical hydrophone, one may introduce an acquisition technique with dual sources towed at different depths in front of the seismic streamer.

The reciprocity principle suggests that the vertical component of particle velocity can be obtained as pressure recording from a source of vertical force. As suggested by Moldoveanu (2000), one practical implementation of a vertical force in the water column is achieved through separate firing of sources towed at different depths (Figure 6).

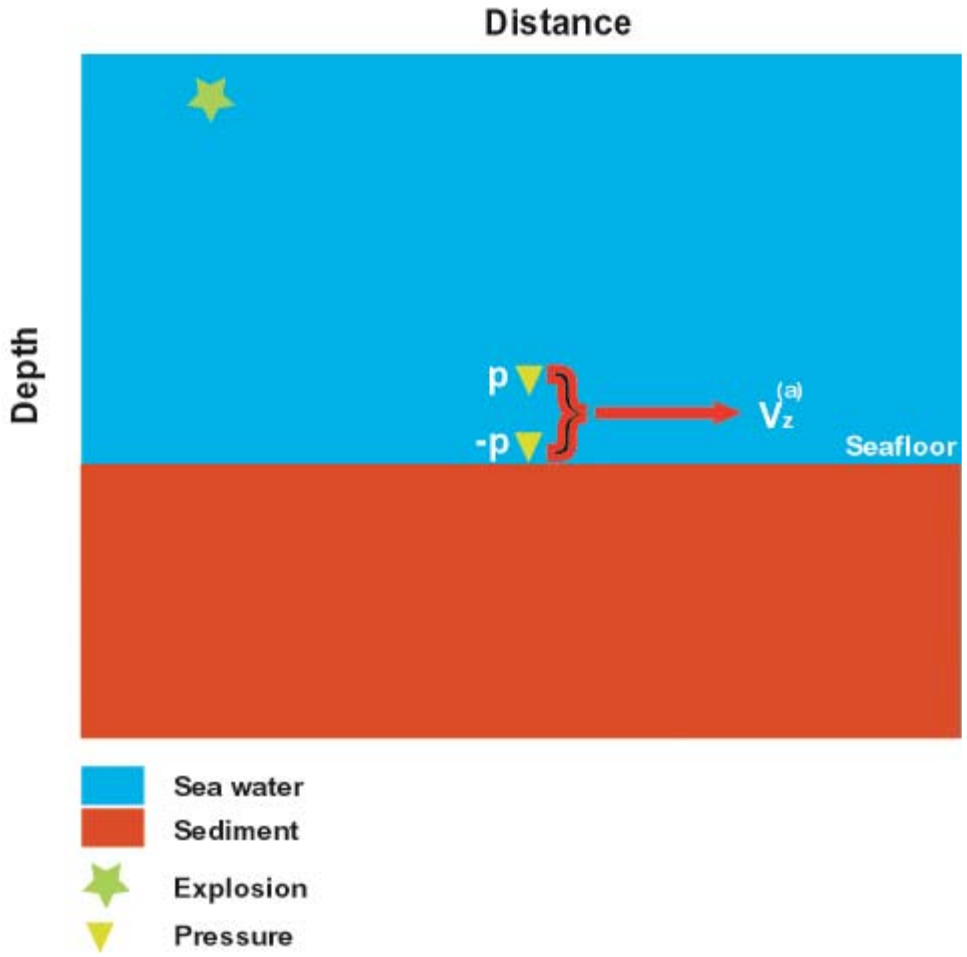

FIG. 5. The vertical component of particle velocity derived from pressure gradient in vertical receiver array experiment.

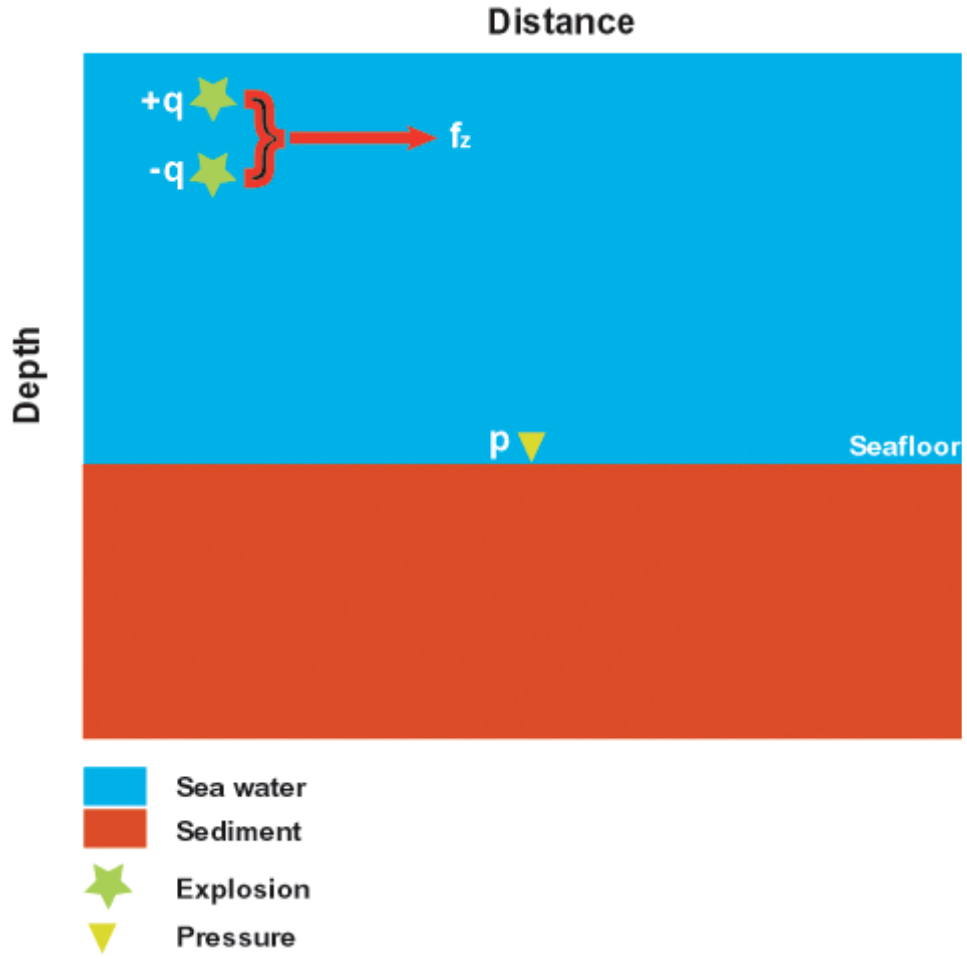

FIG. 6. By setting up marine dipole source, also known as vertical source array, will provide us with another alternative way of measuring the vertical component of the particle velocity.

In Figure 7 hypothetical experiments (source of vertical force, or vertically oriented geophone) and their possible practical realizations are indicated (Figure 8). Figure 9 shows the numerical validation of this result.

Let us recall that the reciprocity principle, i.e.,

$$v_3(x_A,\omega;x_B) = (i\omega)^{-1}\sigma(x_B)p(x_B,\omega;x_A), \tag{7}$$

states that the vertical component of the particle velocity at location x_A due to a monopole point source of volume injection at x_B is identical to the pressure field scaled by the reciprocal of $i\omega$ times density at location x_B from a point force in the vertical direction at x_A.

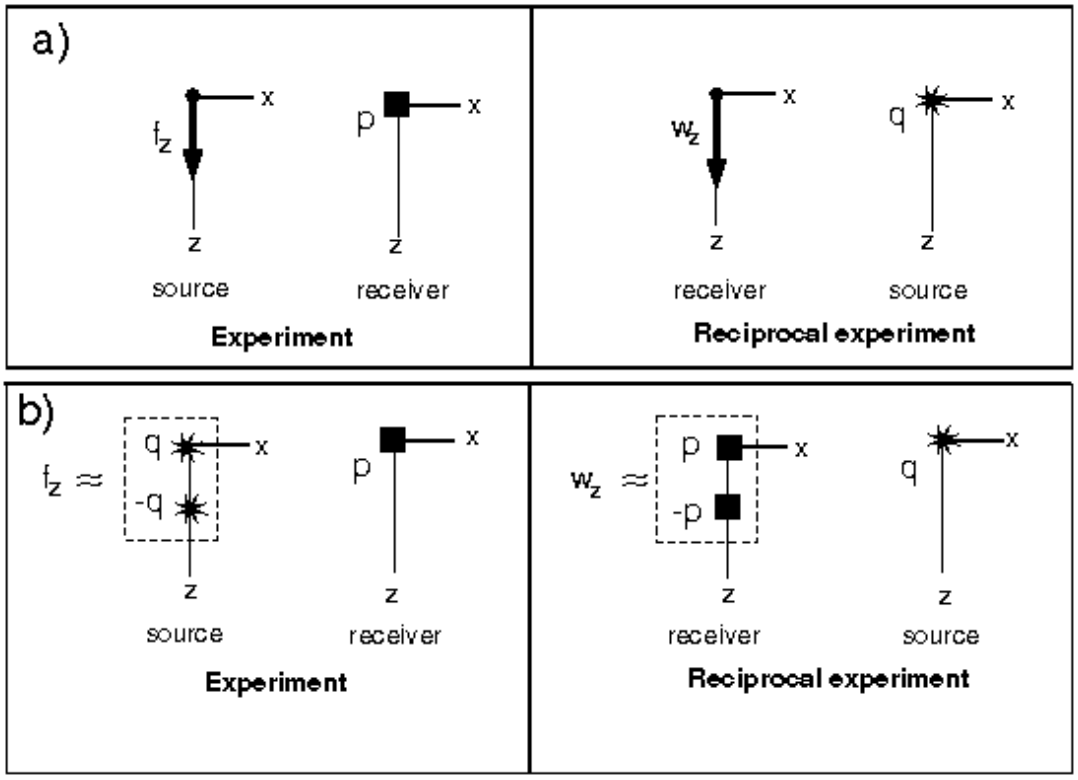

FIG. 7. Reciprocity theorem.

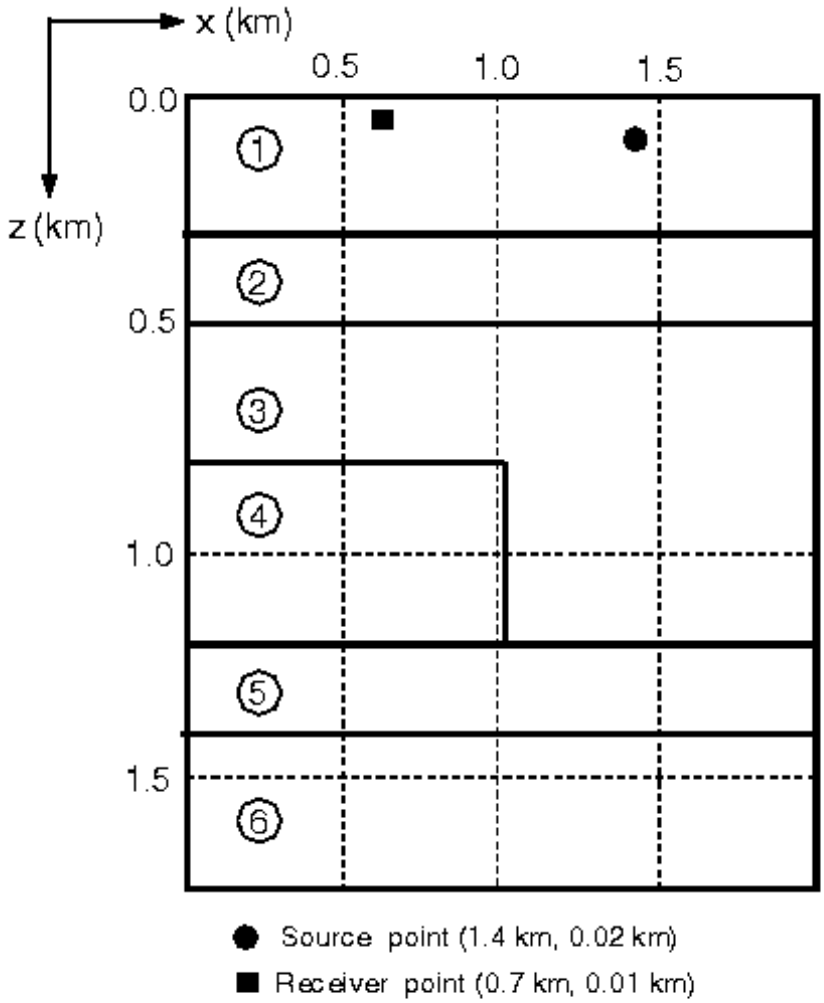

Material	P-wave velocity (m/s)	S-wave velocity (m/s)	Density (g/cc)
1	2000	1000	2.0
2	2200	1300	2.2
3	2600	1450	2.3
4	3000	1700	2.4
5	3800	2100	2.2
6	3600	1700	2.6

FIG. 8. Geological model to prove possible practical realizations of hypothetical experiments in reciprocity theorem.

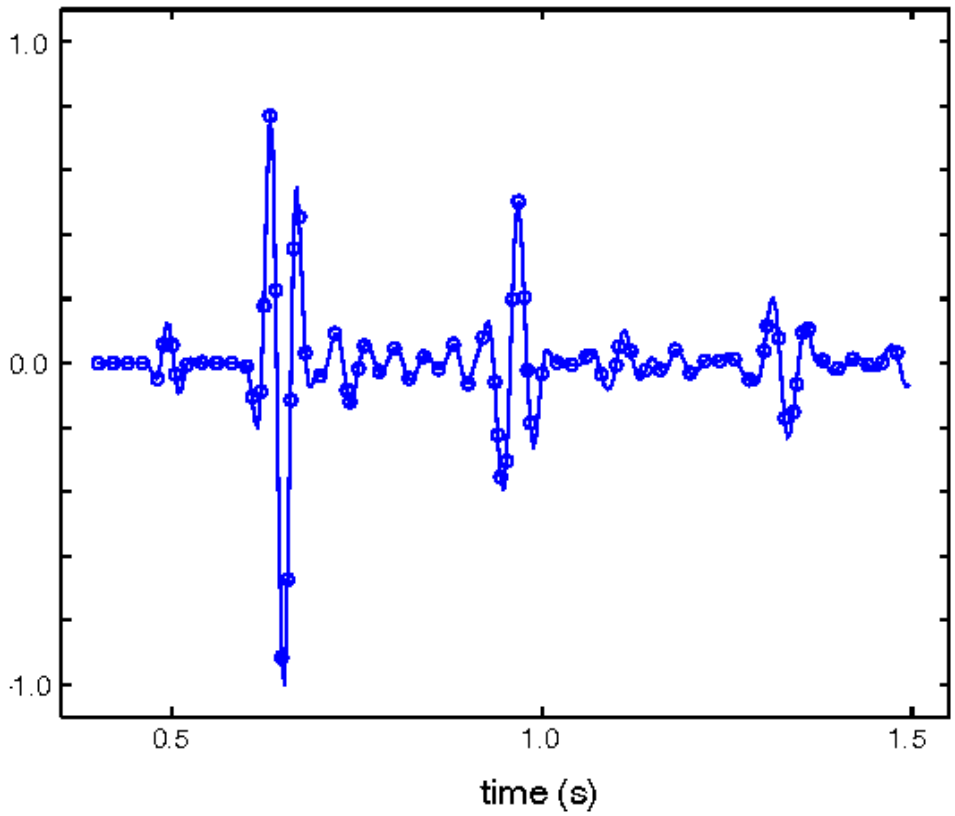

FIG. 9. The numerical validation of reciprocity theorem correspond to geological model in Figure 8. Source (fz) at (1400,10) and receiver (p) at (700,20) is represented by lines. Source (p) at (700,20) and receiver (Vz) at (1400,10) is represented by circles.

BASIC TOOLS USED IN OUR ANALYSIS OF POOR COUPLING

Normalized cross-correlation

To simulate and measure the similarity or time alignment of two traces, three approaches are going to be used. One of them uses normalized cross-correlation between particle velocities. In one instrument, there is always a calibration factor between the measurement just above and below the water. So, we write boundary condition in this form

$$V_z^{(a)}(\omega, x_r) = \alpha(\omega, x_r) V_z^{(b)}(\omega, x_r) \tag{8a}$$

If there is continuity, $\alpha(\omega, x_r)$ will be independent of x_r. The fundamental issue here is to estimate $\alpha(\omega, x_r)$. We proceed as follow

$$V_z^{(b)*}(\omega, x_r) V_z^{(a)}(\omega, x_r) = \alpha(\omega, x_r) V_z^{(b)}(\omega, x_r) V_z^{(b)*}(\omega, x_r) \tag{8b}$$

where the asterisk * denotes a complex conjugate

So we now have an equation which can be used to estimate $\alpha(\omega, x_r)$,

$$\alpha(\omega, x_r) = \frac{V_z^{(b)*}(\omega, x_r)\, V_z^{(a)}(\omega, x_r)}{\varepsilon^2 + \left[V_z^{(b)}(\omega, x_r)\, V_z^{(b)*}(\omega, x_r)\right]} \tag{8c}$$

$\alpha(\omega, x_r)$ is defined as the comparison between the cross-correlation of particle velocity just above and below the seafloor with the auto-correlation of particle velocity below the seafloor. To limited seismic bandwith, we introduce ε^2 to ensure the numerical stability of the estimation of normalized cross-correlation. The arithmetic steps involved in the cross-correlation procedure are not difficult and thus are easily to computer implementation (see flowchart in Figure 10).

Besides normalized cross-correlation, there are two different quantitative approaches we used in combination for identifying such an analysis, consist of total energy ratio and maximum absolute amplitude analysis.

Total energy ratio

Total energy ratio (T_{ar}) is a ratio between total energy of component above the seafloor (a') and below the seafloor (b') as described in equation (10). This ratio value can be used to test for continuity condition. In this experiment, the vertical component of particle velocity (V_z) is mostly used to be analized.

$$a'(x_r) = \sum_t (|V_z^{(a)}(t, x_r)|) \tag{9.a}$$

$$b'(x_r) = \sum_t (|V_z^{(b)}(t, x_r)|) \tag{9.b}$$

$$T_{ar} = \frac{a'(x_r)}{b'(x_r)} = \frac{\sum_t (|V_z^{(a)}(t, x_r)|)}{\sum_t (|V_z^{(b)}(t, x_r)|)} \tag{10}$$

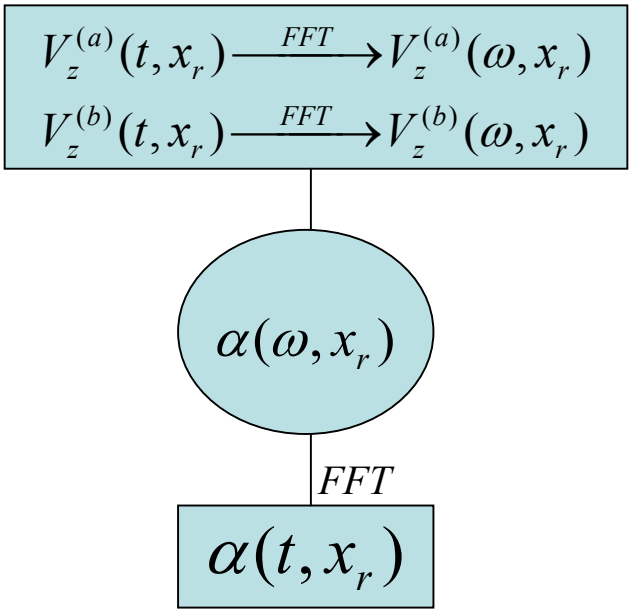

FIG. 10. The arithmetic steps involved in the cross-correlation procedure. Fast Fourier Transfrom (FFT) is used during time-frequency domain processing.

Maximum absolute amplitude

The maximum absolute amplitude which represents the first reflection amplitude, can also be used as a diagnostic tool to investigate the nature of the seafloor reflector.

$$a(x_r) = \underset{t}{Max}(|V_z^{(a)}(t, x_r)|) \tag{11.a}$$

$$b(x_r) = \underset{t}{Max}(|V_z^{(b)}(t, x_r)|) \qquad (11.b)$$

In most cases, we use the cross-correlation and the total energy for detecting poor coupling. However, we also can use cross-correlation and maximum absolute amplitude to investigate dipping seafloor effect.

CHAPTER III

DETECTING POOR COUPLING ON SYNTHETIC FINITE-DIFFERENCE METHOD DATA

FINITE-DIFFERENCE METHOD

Introduction

Many interests in the extraction of fine detail from field seismograms has encouraged the search from numerical modeling procedures which can generate synthetic seismograms for subsurface geometries and for arbitrary source-receiver separations. Among the various techniques available for this purpose, the finite-difference techniques are by far most precise way of simulating elastic wave propagation through complex media provided that the grid spacing is chosen properly (Kelly et al., 1976). Finite-difference modeling (FDM) can accurately predict travel times and amplitudes of primaries, multiples, converted waves and diffractions, and hence, closely simulate the real earth's response.

Partial differential equations of the wave motion is solved by the finite-difference technique. The derivatives are approximated by a truncated Taylor series whose accurateness depends essentially on the sampling of the geological model. Our objective here is to validate the accuracy of the CASP finite-difference software used for OBS experiment data.

Elastic wave equations

The elastic wave equations to be solved by using our finite-difference software are as follows (Virieux, 1986):

$$\rho \frac{\partial u_t}{\partial t} = \frac{\partial \tau_{xx}}{\partial_x} + \frac{\partial \tau_{xz}}{\partial_z} \tag{12}$$

$$\rho \frac{\partial w_t}{\partial t} = \frac{\partial \tau_{zx}}{\partial_x} + \frac{\partial \tau_{zz}}{\partial_z} \tag{13}$$

$$\tau_{xx} = (\lambda+2\mu)\frac{\partial u}{\partial x} + \lambda \frac{\partial w}{\partial z} \tag{14}$$

$$\tau_{zx} = \mu\left(\frac{\partial u}{\partial z} + \frac{\partial w}{\partial x}\right) \tag{15}$$

$$\tau_{zz} = (\lambda+2\mu)\frac{\partial w}{\partial z} + \lambda \frac{\partial u}{\partial x} \tag{16}$$

In these equations, u_t and w_t are the horizontal and vertical particle velocity respectively, u and w are the horizontal and vertical displacement components respectively, τ_{xx}, τ_{zx}, and τ_{zz} are the stress tensors, ρ is the density, λ and μ are the Lame' parameters.

Finite-difference technique

The finite-difference method operates by replacing the derivatives in an equation by finite-differences. If we consider a function, *f(x)*, its Taylor's Theorem expansion about x can be written as

$$f\left(x+h\right) = f\left(x\right) + hf'(x) + \frac{h^2}{2}f''(x) + \frac{h^3}{6}f'''(x) + \ ..., \tag{17}$$

or, alternatively,

$$f\left(x+h\right)=f\left(x\right)-hf'(x)+\frac{h^2}{2}f''(x)-\frac{h^3}{6}f'''(x)+\ ..., \tag{18}$$

Here, h is the spatial increment. If h is small, the higher-order terms will become negligible. If we truncate the series in equations (17) and (18) after the third term, the first derivative of *f(x)* can be solved by

$$f'\left(x\right)=\frac{1}{h}\left[f\left(x+h\right)-f\left(x\right)\right]-\frac{h}{2}f''(\xi_1) \tag{19}$$

and

$$f'\left(x\right)=\frac{1}{h}\left[f\left(x\right)-f\left(x+h\right)\right]-\frac{h}{2}f''(\xi_2) \tag{20}$$

respectively, $\frac{h}{2}f''(\xi)$ where is the truncation error term. Equations (14) and (15) lead to the finite-difference approximations

$$f'\left(x\right)\approx\frac{1}{h}\left[f\left(x+h\right)-f\left(x\right)\right] \tag{21}$$

and

$$f'\left(x\right)\approx\frac{1}{h}\left[f\left(x\right)-f\left(x+h\right)\right] \tag{22}$$

The expressions contained in the [] on the right hand side of equations (21) and (22) are called finite-differences. Equations (21) and (22) are considered first-order accurate with an error of *O(h)* because the truncation error term is first order with respect to h.

Alternatively, the truncation and subtraction of equations (17) and (18) yields

$$f'\left(x\right)=\frac{1}{2h}\left[f\left(x+h\right)-f\left(x-h\right)\right]-\frac{h^2}{6}f'''(\psi) \tag{23}$$

where $\psi=\xi_1+\xi_2$ .This leads to the second-order approximation

$$f'(x) \approx \frac{1}{2h}\left[f(x+h) - f(x-h)\right] \tag{24}$$

with error O(h^2) (truncation error term is second order, h^2). This approximation is more precise and favorable compared to the approximations in equations (21) and (22). By retaining terms in the Taylor expansion series, higher order approximations are possible and precision increases. References to higher-order approximations can be visited in Bayliss et al. (1986), Dablain (1986), and Levander (1988).

Implementation

This finite-difference software requires finite-difference computations with respect to time and space. For the temporal derivatives, we use a second-order approximation given by

$$f'(t) \approx \frac{1}{2t}\left[f(t+\Delta t) - f(t-\Delta t)\right] \tag{25}$$

For the spatial derivatives, we use a fourth-order approximation given by

$$f'(x) \approx \frac{1}{2\Delta x}\left[f(x+\Delta x) - f(x-\Delta x)\right] - \frac{\Delta x^2}{6} f'''(x) \tag{26}$$

where Δt is the temporal increment and Δx is the spatial increment. Higher-order finite-difference approximations improve precision and reduce the spatial sampling necessary to accurately simulate wave propagation, therefore reducing computation time and memory requirements (Levander, 1988).

The finite-difference software uses a staggered grid in both space and time (Levander, 1988; and Virieux,1986), as seen in Figure 11, to update velocity and stress

calculations. The points at which the stresses are specified are halfway between the points at which the velocities are specified. So in one time step, both the velocity and stress component are updated. The spatial finite-difference is derived using four points adjacent to the location being updated. If the normal stress variable is being updated, the four adjacent velocity nodes are used. This allows differences that are naturally centered at the required point.

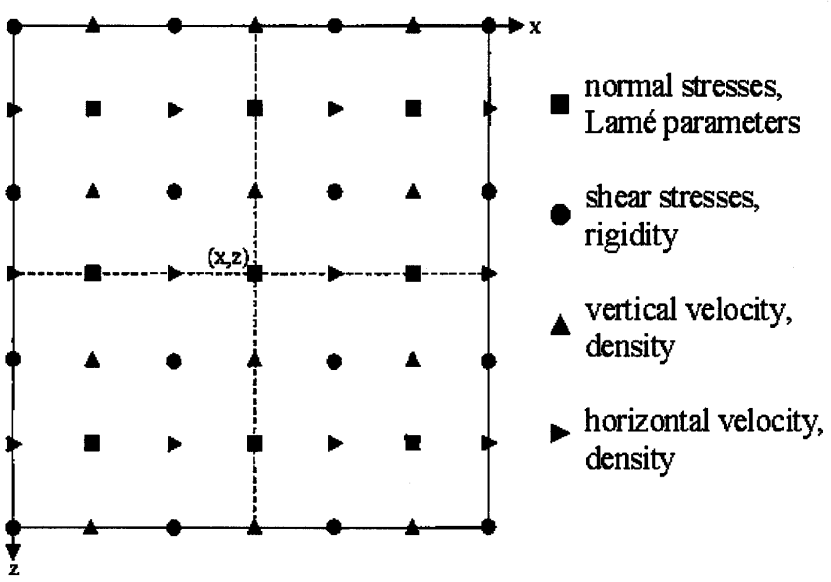

FIG. 11. Finite-difference staggered grid used to update the velocity and stress calculations (modified from Levander, 1988).

The benefit of the staggered grid scheme which is used in our FDM software include (1) stability for all values of Poisson's ratio, (2) minimized grid dispersion and grid anisotropy, (3) ability to simulate surface or buried sources, and (4) ability to

simulate free-surface boundary conditions (see Levander (1988) for more discussion these benefits).

ACCURACY OF FDM IN OBS EXPERIMENT

Setting up finite-difference experiment

Based on continuity condition as described by equation (8a), we have to adjust receiver position with regard to depth properly, so we may accurately modeling bottom of the water in the seafloor and top of the sediment. Since we used finite-difference method to simulate our modeling, grid spacing has to be an important parameter that we have to dealt with. Due to finite-difference gridding of the geological model, the receiver can not be located exactly at the seafloor.

We decided to work on fourth-order spatial difference stencils in a finite-difference staggered grid for modeling marine problem accurately. Receiver has to be placed at least 3 points above the seafloor to ensure that our measurements are carried out in the water without interference with the solid. Similarly, the receiver below the seafloor must be placed at least 3 points below the seafloor to ensure that our measurements are carried out in the solid without interference with the water in the finite-difference staggered grid (Figure 12).

The seafloor ghost has to be another issue that we have to dealt with (Figure 12). As the increasing of point above the seafloor in the grid, the effect of the seafloor ghost will be bigger. This effect has to be reduced and must be small.

We end up putting receiver 4 points above the seafloor for the pressure field and 4 points below the seafloor for recording pressure and the particle velocity in this thesis.

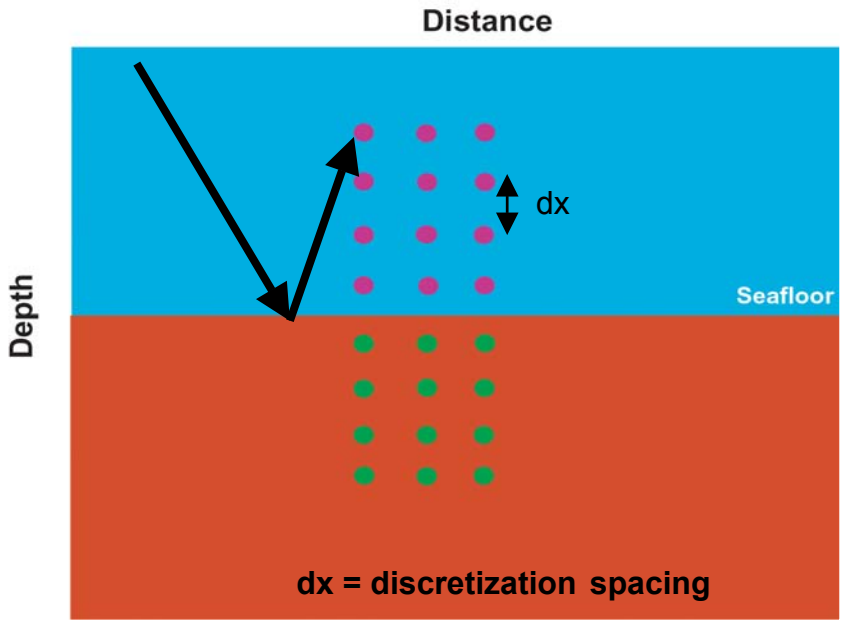

FIG. 12. Issues to be dealt with in setting up finite-difference in OBS experiment.

Data generated by finite-difference method modeling

Five numerical experiments are performed to explore the methodology for setting up finite-difference modeling for acoustic-elastic cases.

Geological Modeling 1 and 2 (Figures 13 and 14) to experiment suitable grid spacing for acoustic-elastic case in an OBS experiment and explore its relationship to finite-difference modeling. Geological modeling 3 (Figure 15) looks into the effect of varying dip in the seafloor. Geological modeling 4 (Figure 16) is used to investigate

discreet contrast in seafloor topography. Geological modeling 5 (Figure 17) included complex subsurface geology beneath the seafloor.

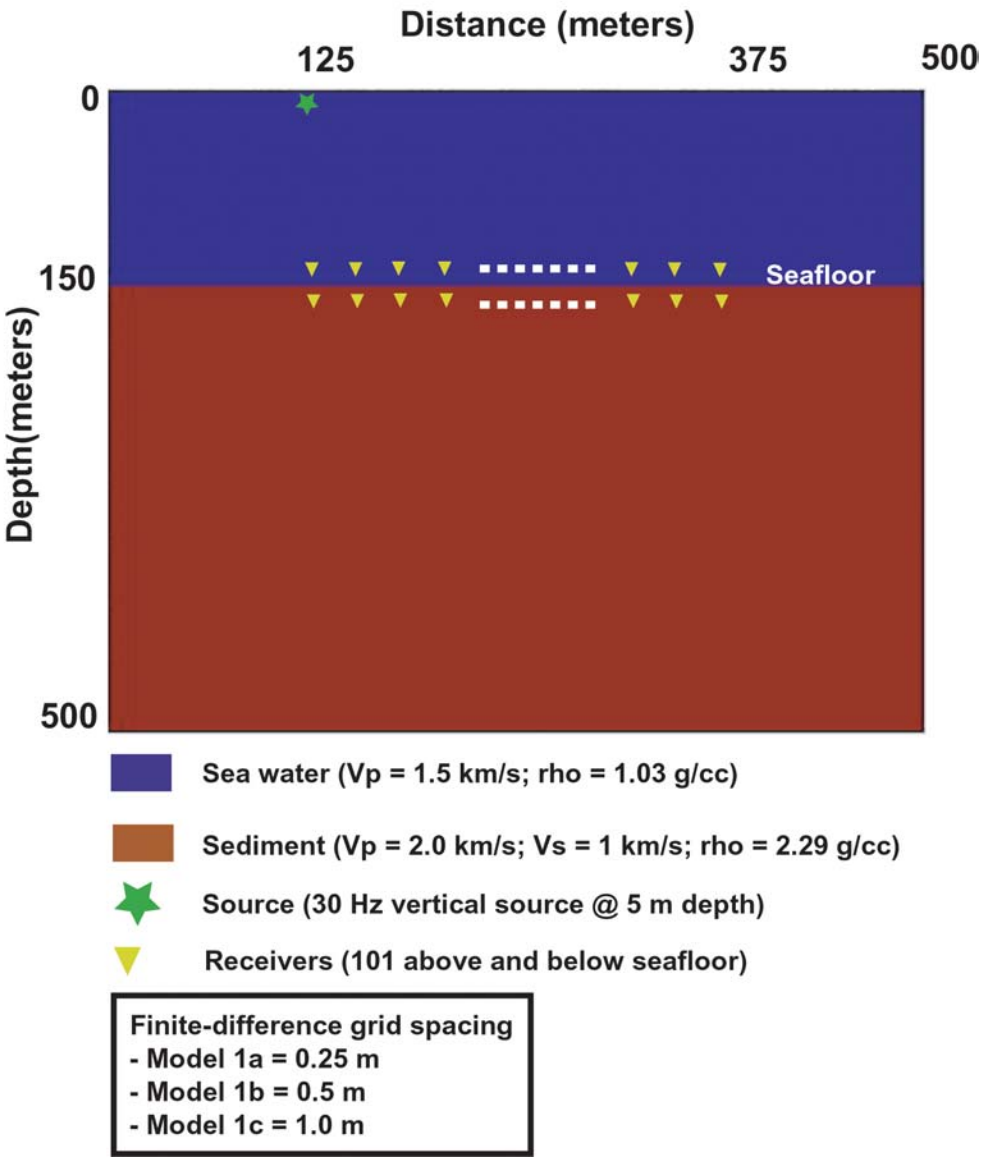

Fig. 13. Geological model 1 (flat single layer) correspond to grid points 2000 X 2000.

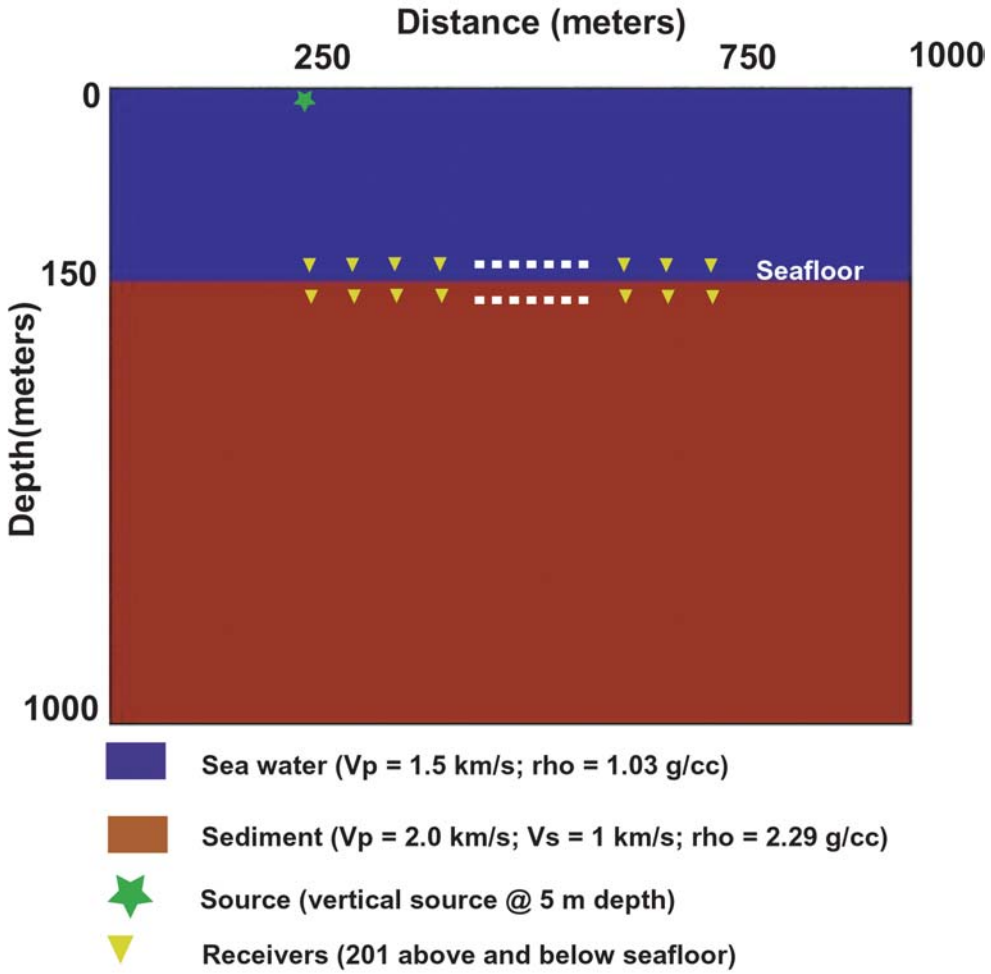

FIG. 14. Geological model 2 (flat single layer) correspond to grid points 4000 X 2000.

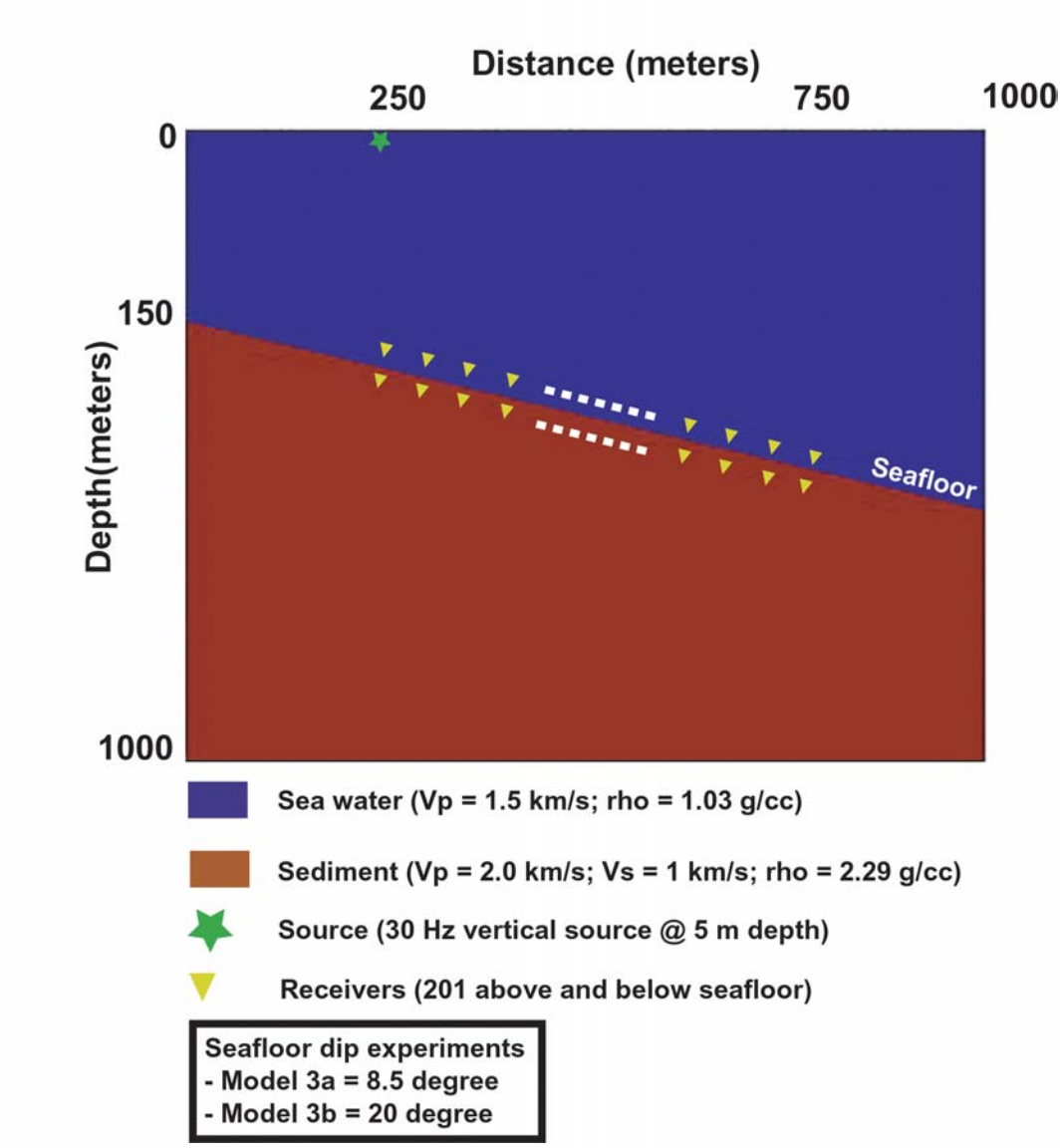

FIG. 15. Geological model 3 (dipping single layer) correspond to grid points 4000 X 2000.

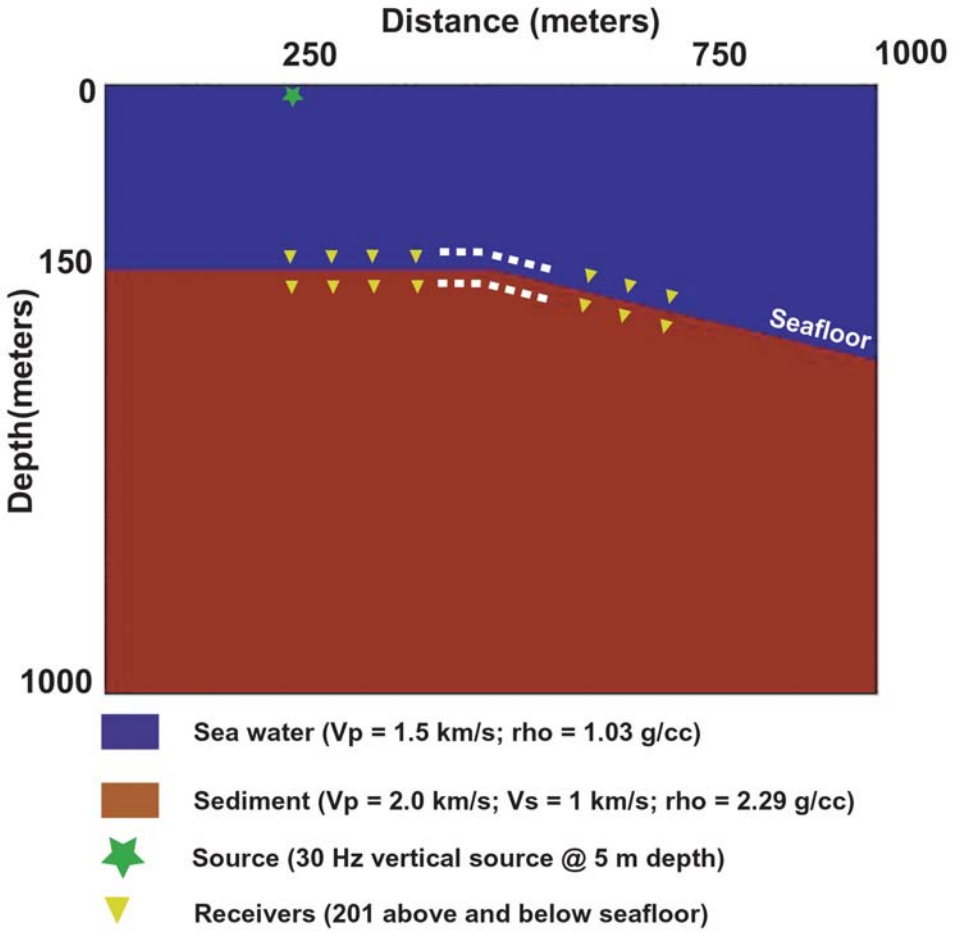

FIG. 16. Geological model 4 (half flat-half dipping single layer) correspond to grid points 4000 X 2000.

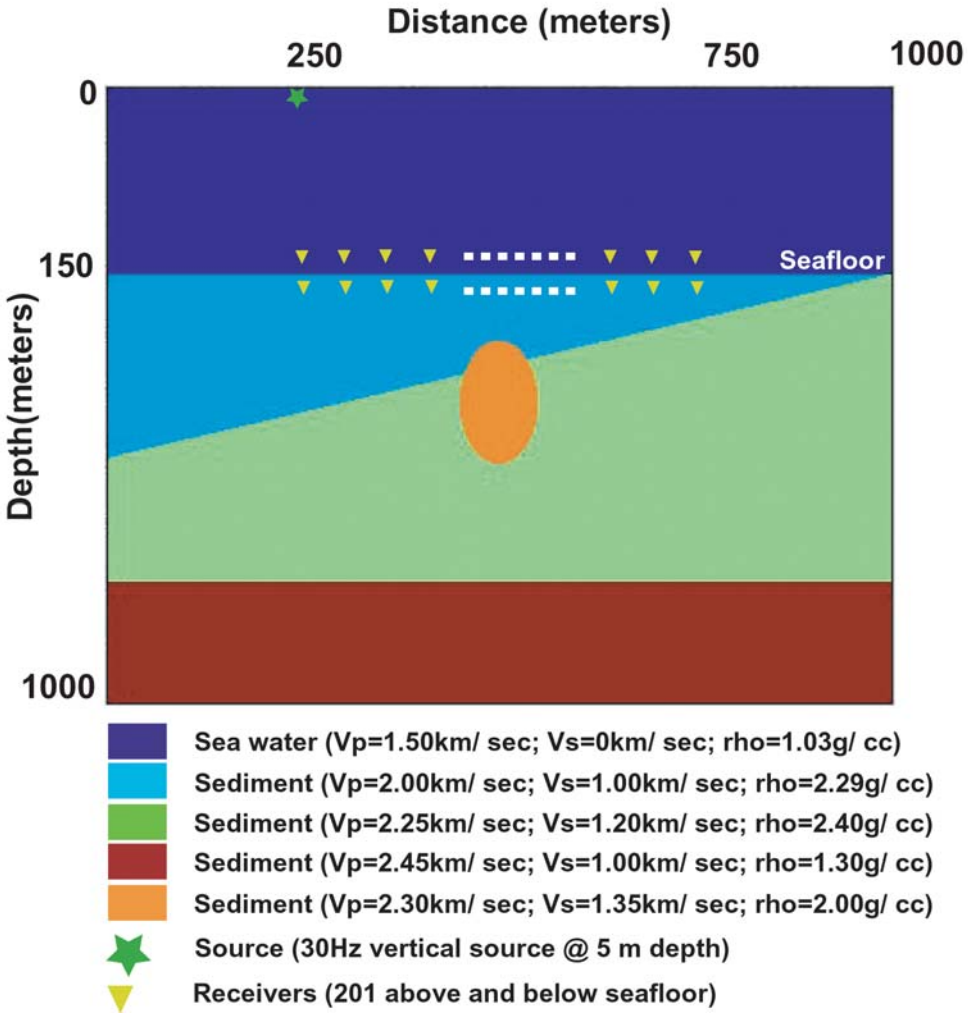

FIG. 17. Geological model 5 (complex subsurface geology) correspond to grid points 4000 X 2000.

The grid spacing is an important issue while setting up the numerical experiment as continuity condition needs to be satisfied as close as possible. The continuity conditions can be tested by examining the total energy (Figure 18) and maximum absolute amplitude (Figure 19). In case the continuity condition is perfectly satisfied then the total energy ratio will be closed to 1 and maximum absolute amplitude values

will be similar for geophones above and below the seafloor. Comparing Figure 18 clearly shows that with grid spacing of 0.25 m (blue curve), the continuity condition is best satisfied. When the grid spacing is increased {0.5 m (pink curve) and 1 m (red curve)}, the amplitudes above the seafloor increasing magnitude because of significant contribution of receiver ghost. The shot gathers for model 1a is shown in Figure 20.

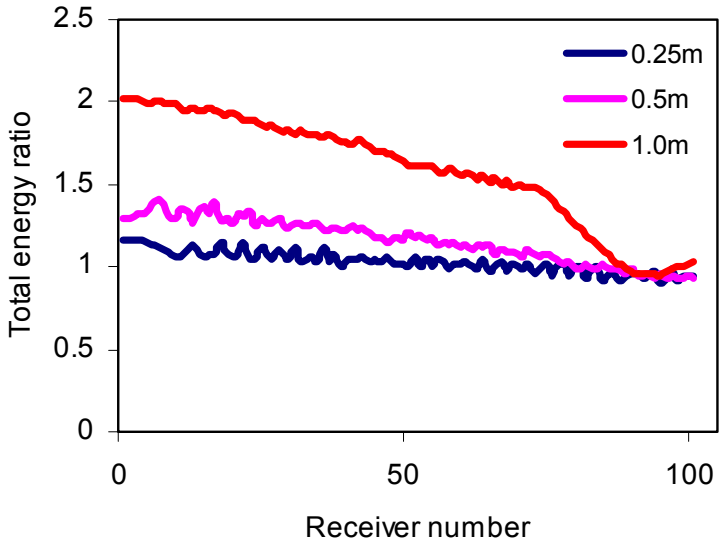

FIG. 18. Total energy ratio of geological model 1 (flat single layer) between Vz (above seafloor) and Vz (below seafloor). Three different synthetic finite-difference modeling data are generated correspond to grid spacing 0.25m, 0.5m, and 1m.

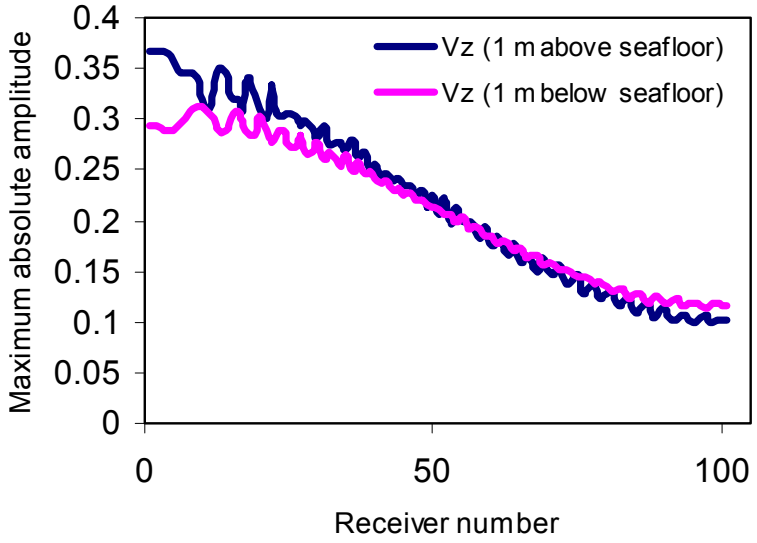

FIG. 19. Maximum absolute amplitude between Vz (above seafloor) and Vz (below seafloor) of geological model 1 (flat single layer) with 0.25m discretization spacing.

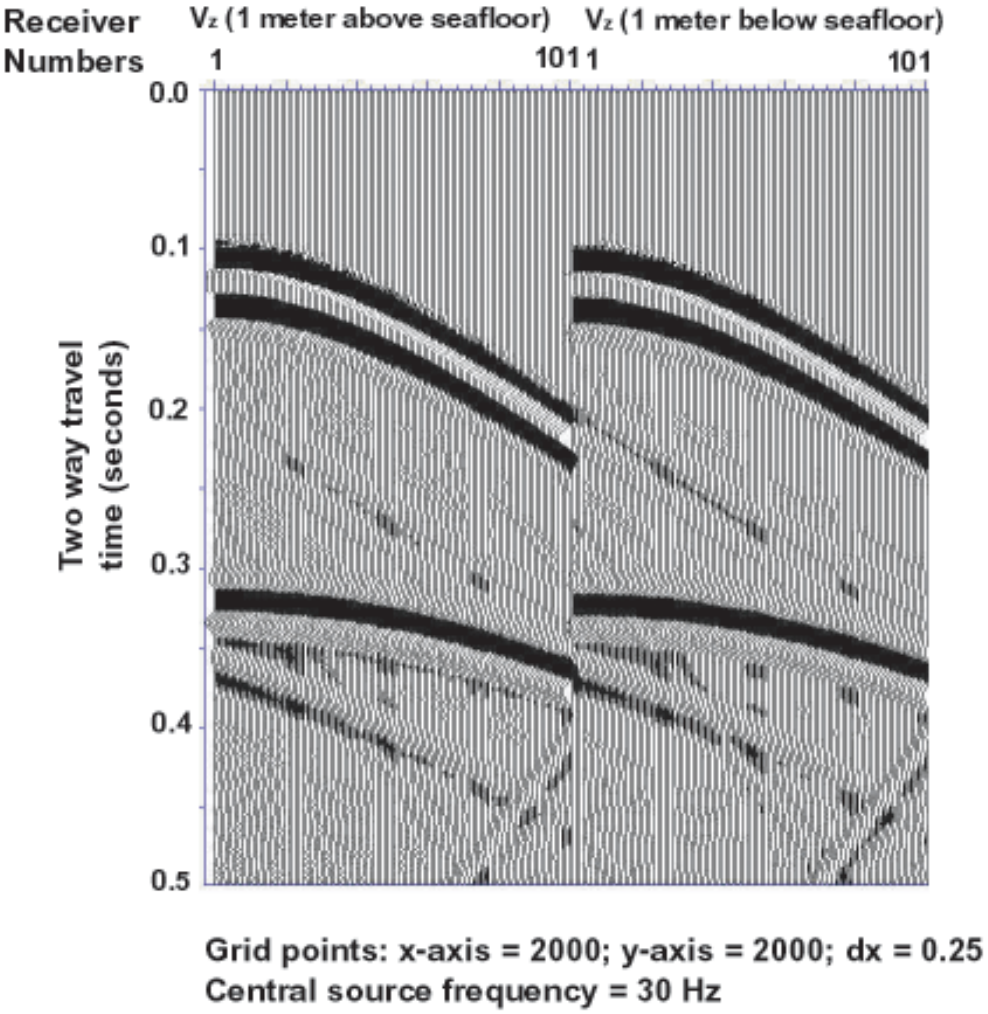

FIG. 20. Shot gathers for Vz component of geophones for geological model 1 (flat single layer) with 0.25m discretization spacing.

DETECTING POOR COUPLING

Poor coupling happens when geophone is not firmly planted into the seafloor (Figure 2). Here, I assume that the geophone is properly calibrated but since is not physically attached to the seafloor in the proper manner the poorly coupled geophone is partly acting like a hydrophone.

One way of simulating poor coupled geophone by picking up a pressure component trace and placing it in the vicinity of particle velocity component traces (Figure 21).

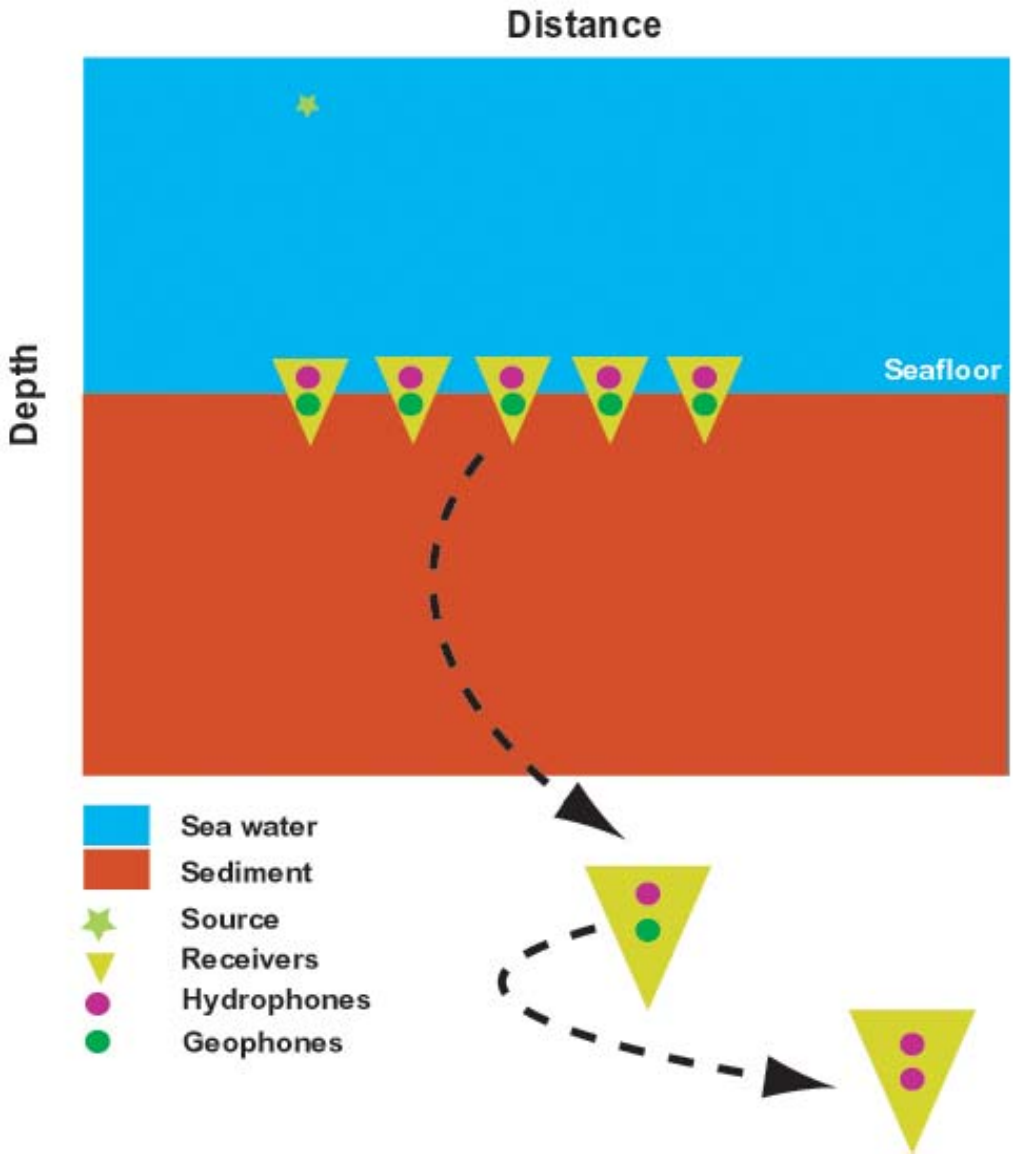

FIG. 21. Methodology presented to simulate poor coupling.

Geological model 2 was used as a test case to examine the effect of poor coupling. A poorly coupled geophone has a similar amplitude compared to other geophone in the vicinity (Figure 22), but has the phase difference as it acts like a hydrophone in some sense (Figures 23).

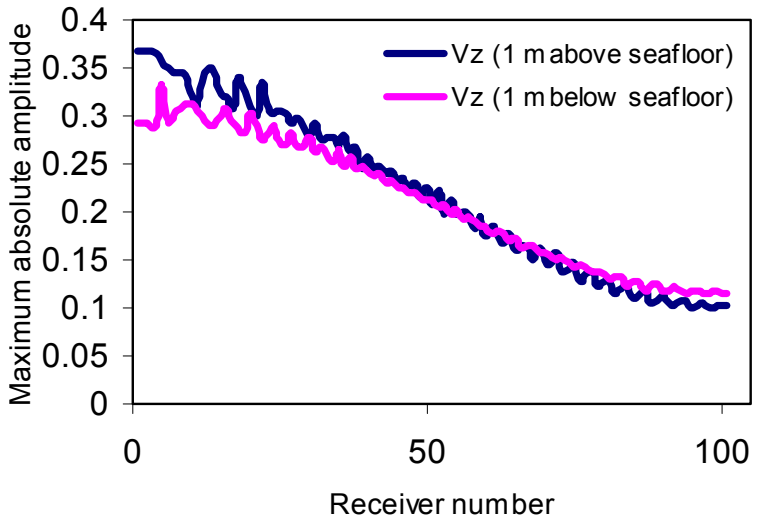

FIG. 22. Maximum absolute amplitude between Vz (above seafloor) and Vz (below seafloor) for poor coupling case of geological model 2 (flat single layer).

Normalized cross-correlation plot (Figure 24) has been used to develop diagnostic tools to identify poor coupling. Figure 24 shows very distinctive signature of maximum correlation value being offset in time lag for poorly coupled trace.

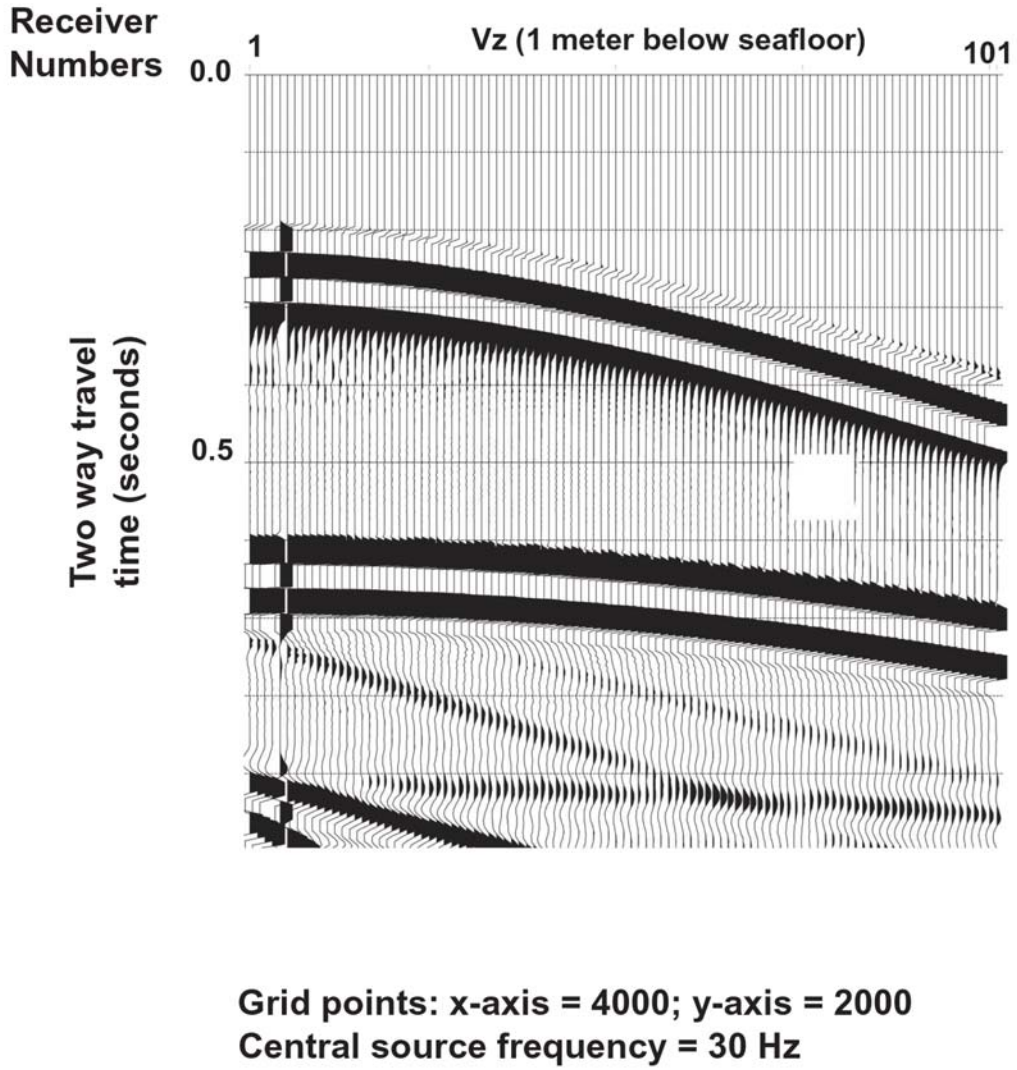

FIG. 23. Shot gather for Vz component of a poor coupled geophone for geological model 2 (flat single layer) with 0.25m discretization spacing. Poor coupling trace at receiver number 5.

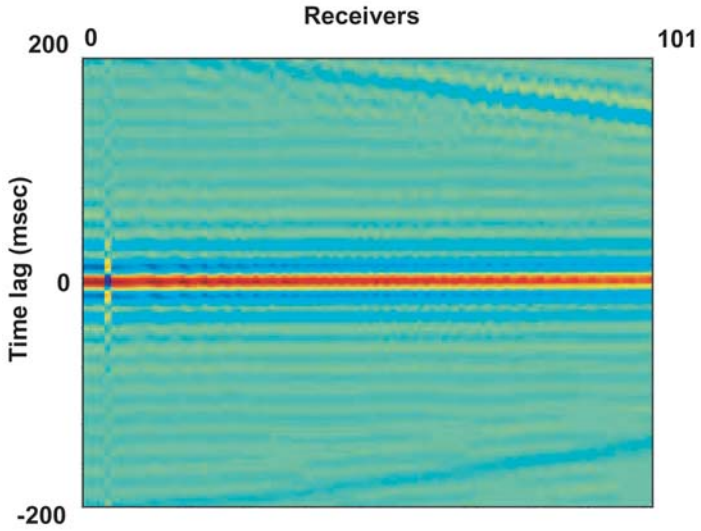

FIG. 24. Normalized cross-correlation between Vz (above seafloor) and Vz (below seafloor) for geological model 2 (flat single layer) correspond to poor coupling case.

DIFFERENTIATING THE EFFECTS OF SEAFLOOR TOPOGRAPHY AND BAD DATA WITH REGARDS TO POOR COUPLING

Numerical experiments are conducted for different seafloor dips, sudden change in seafloor topography, and other data problems. Here, an attempt is made to uniquely identify diagnostic tools including normalized cross-correlation and amplitude analysis for each case. Then to know how they measure up in our diagnostic tools analysis with regard to poor coupling.

Detecting and correcting for local orientation of geophone

An important consequence of examining amplitude geophone values above and below the seafloor is that one can develop diagnostic tools to detect local orientation of

the coupling. A real seafloor contains a large number of a sudden change in topography even tough those changes might be small in scale with respect to the width.

Experiment here shown for dipping seafloor (Figure 15) clearly demonstrate that the continuity condition start diverging when the geophone is not oriented perfectly perpendicular. The shot gathers for this model is shown in figure 25. The continuity condition for geophone above and below the seafloor starts diverging apart in the dipping seafloor and the magnitude of the divergence increases when dip of the seafloor is increased from 8.5 degrees (pink curve) to 20 degrees (red curve) as shown in Figures 26. Local changes in dip of the seafloor can be identified in similar way as we identified the divergence of continuity condition with respect to regional changes in the dip. An interesting observation is that the divergence in the continuity condition increases with the dip. This could be used in a qualitative way to identify varying local dips on the seafloor.

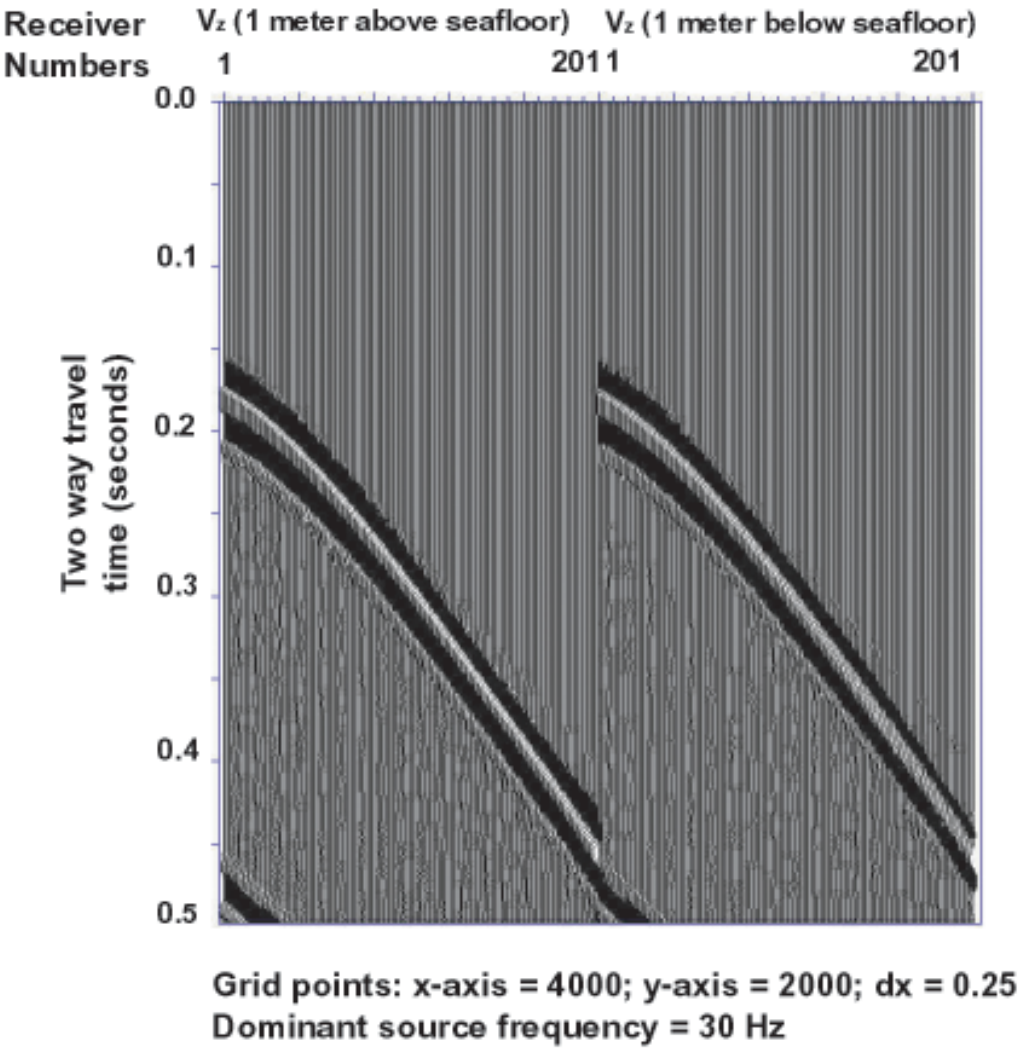

FIG. 25. Shot gathers for Vz component of geophones for geological model 3 (single layer with dip 8.5^{o}) with 0.25m discretization spacing.

Figure 26 may also distinguish between downdip case and updip case. Here, reverse curve gradient can be used to differentiate among them, where positive gradient

(pink curve) represents downdip case and negative gradient (gray curve) represents updip case.

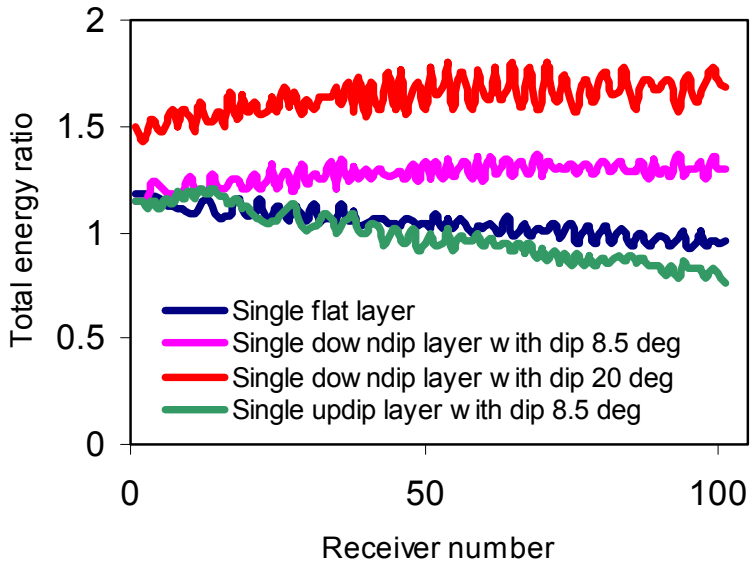

FIG. 26. Total energy ratio between Vz (above seafloor) and Vz (below seafloor) for geological model 1, model 3 (downdip, 8.5 deg), model 3 (downdip, 20 deg), and updip (8.5 deg) model.

Figure 16 and Figure 27-29 show that one can identify sudden changes in the dip of the seafloor by investigating the amplitudes of geophone above and below the seafloor. In this example, sudden changes is begun at receiver number 101.

In Figure 17 and Figures 30-31, one can see that the effect of complex subsurface geology does not have any effect on the continuity condition for geophone above and below the seafloor.

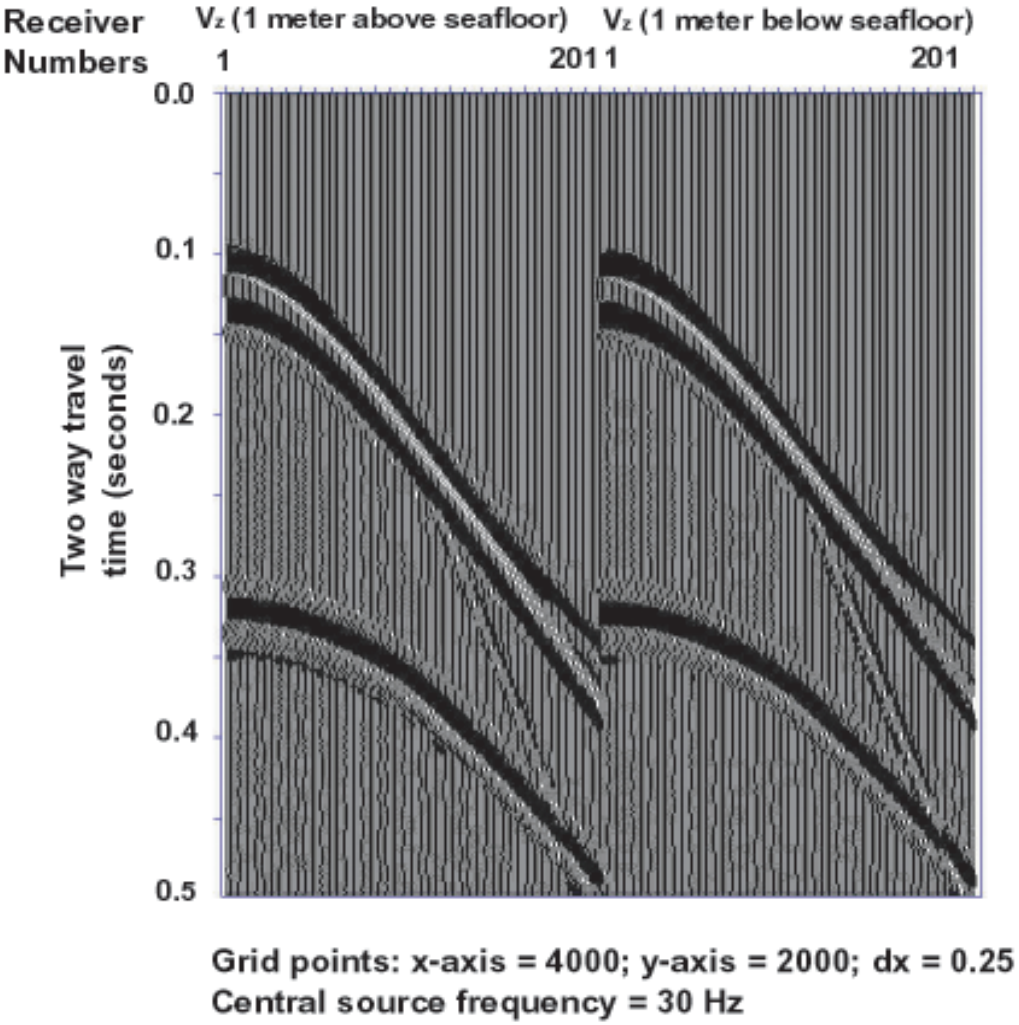

FIG. 27. Shot gathers for Vz component of geophones for geological model 4 (half flat-half dipping) with 0.25m discretization spacing.

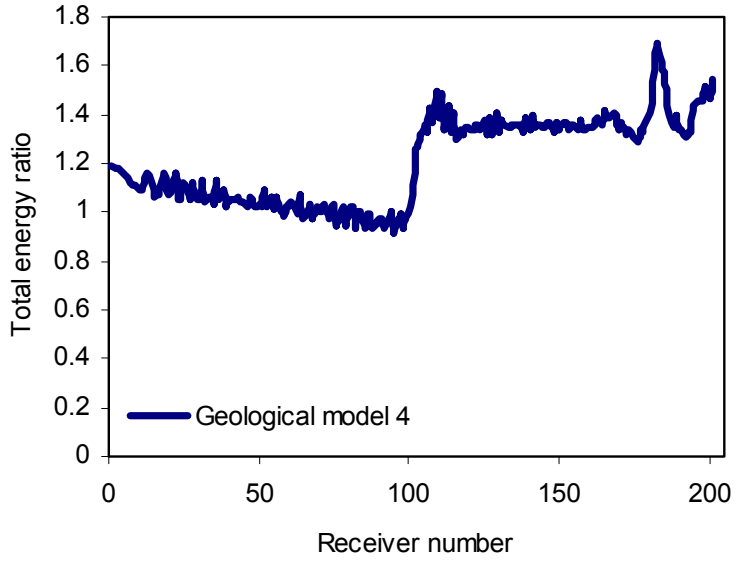

FIG. 28. Total energy ratio between Vz (above seafloor) and Vz (below seafloor) of geological model 4 (half flat-half dipping single layer).

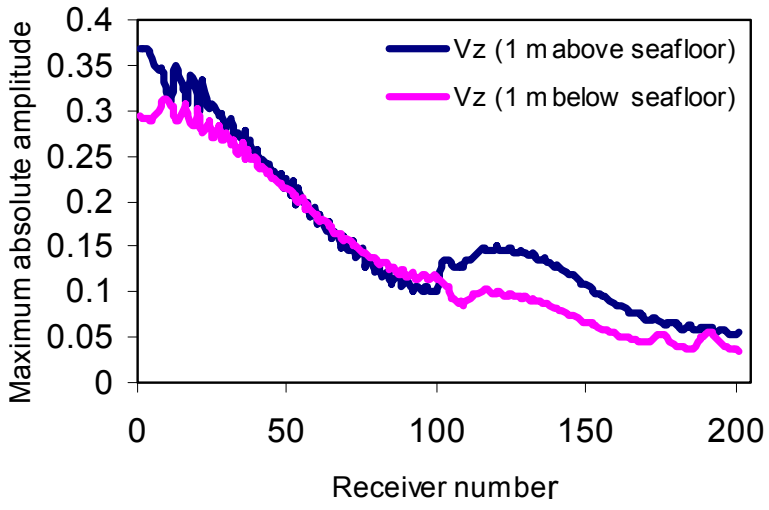

FIG. 29. Maximum absolute amplitude between Vz (above seafloor) and Vz (below seafloor) of geological model 4 (half flat-half dipping single layer).

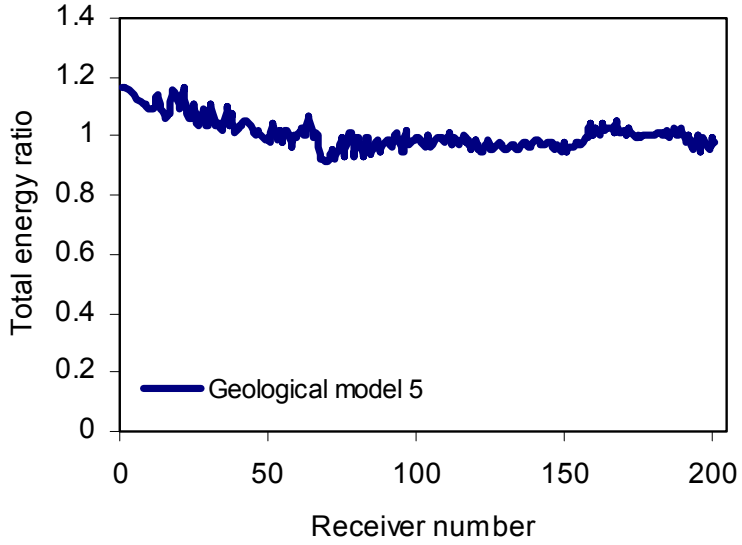

FIG. 30. Total energy ratio between Vz (above seafloor) and Vz (below seafloor) of geological model 5 (complex subsurface geology model).

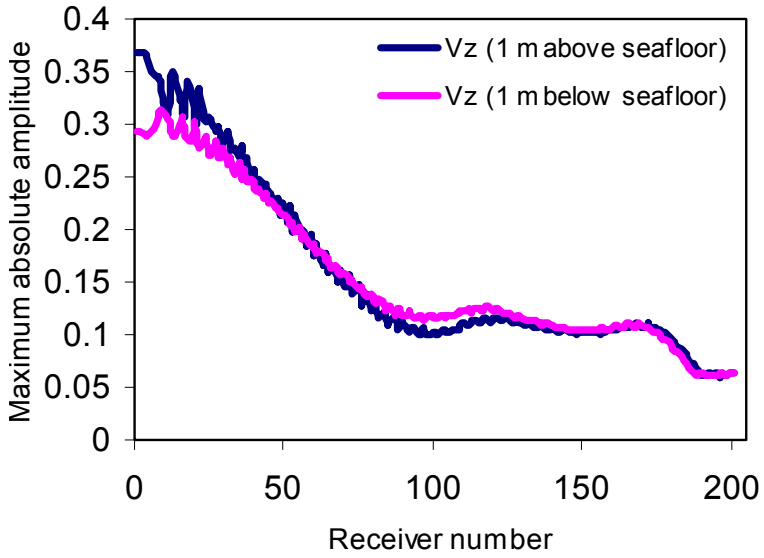

FIG. 31. Maximum absolute amplitude between Vz (above seafloor) and Vz (below seafloor) of geological model 5 (complex subsurface geology model).

Differentiating bad data with regards to poor coupling

Our methodology for detecting poor coupling is to set up scenarios for poor coupling, bad traces and dim traces. Geological model 2 was used as a test case to examine the effect of poor coupling, bad trace and dim trace. Poor coupling was distinguished with bad traces and dim traces in the falling manner: (1) A poorly coupled geophone has a similar amplitude compared to other geophone in the vicinity, but has the phase difference as it acts like a hydrophone in some sense (Figures 22 - 24); (2) A dim trace is where the calibration of geophone is off and amplitude is not similar to the geophone in the vicinity (Figures 32 - 34); (3) A bad trace is caused when the geophone stops functioning during the survey. Therefore, no recording is made at the geophone (Figures 35 - 37).

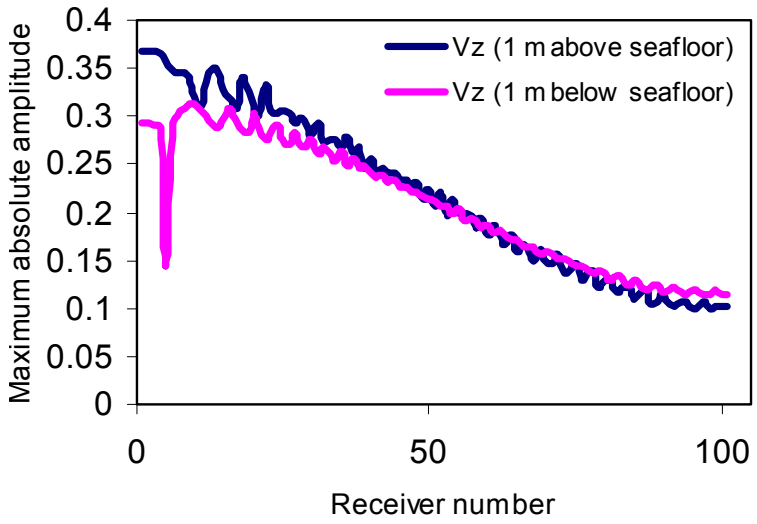

FIG. 32. Maximum absolute amplitude between Vz (above seafloor) and Vz (below seafloor) of geological model 2 (flat single layer) for dim trace case.

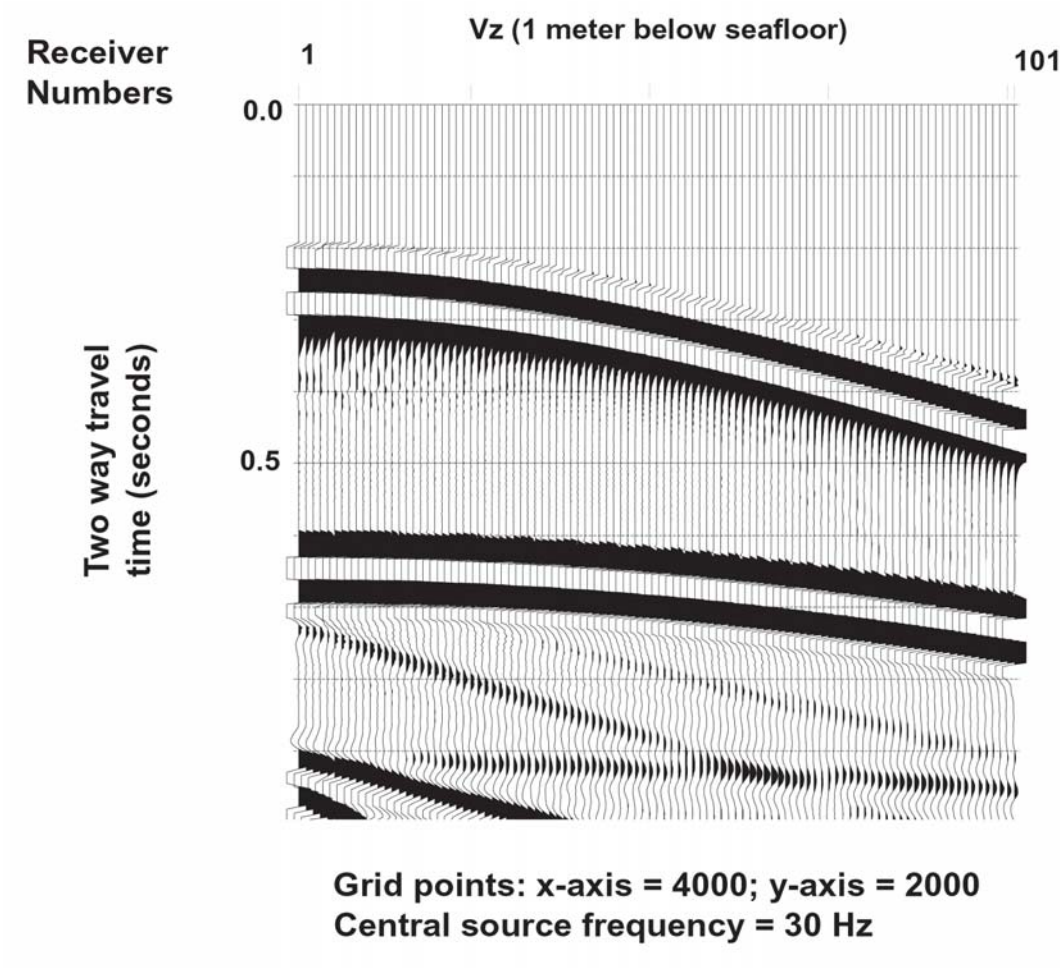

FIG. 33. Shot gather for Vz component of a dim coupled geophone for geological model 2 (flat single layer model) with 0.25m discretization spacing. Dim trace at receiver number 5.

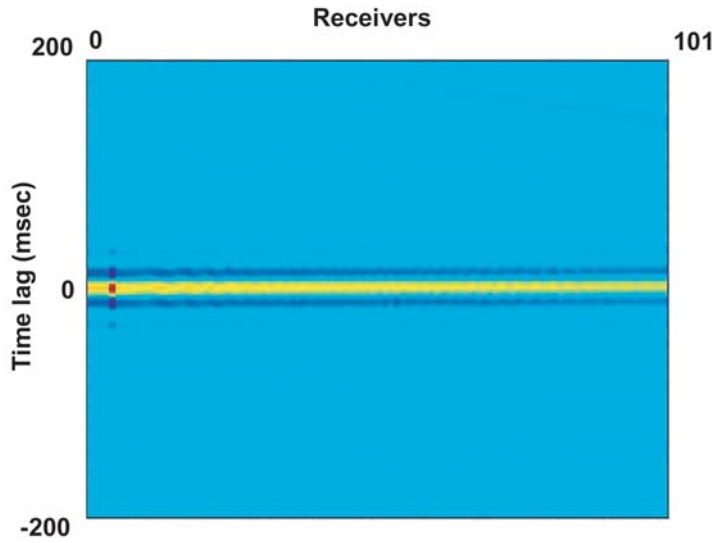

FIG. 34. Normalized cross-correlation between Vz (above seafloor) and Vz (below seafloor) for geological model 2 correspond to dim trace case.

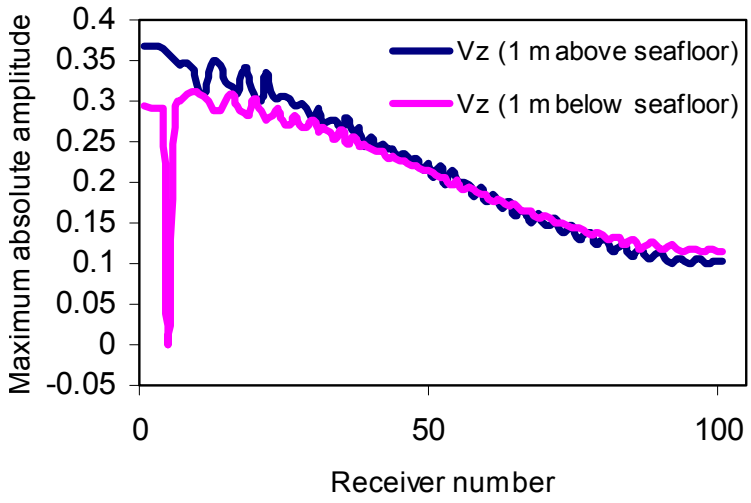

FIG. 35. Maximum absolute amplitude between Vz (above seafloor) and Vz (below seafloor) of geological model 2 (flat single layer) for zero trace case.

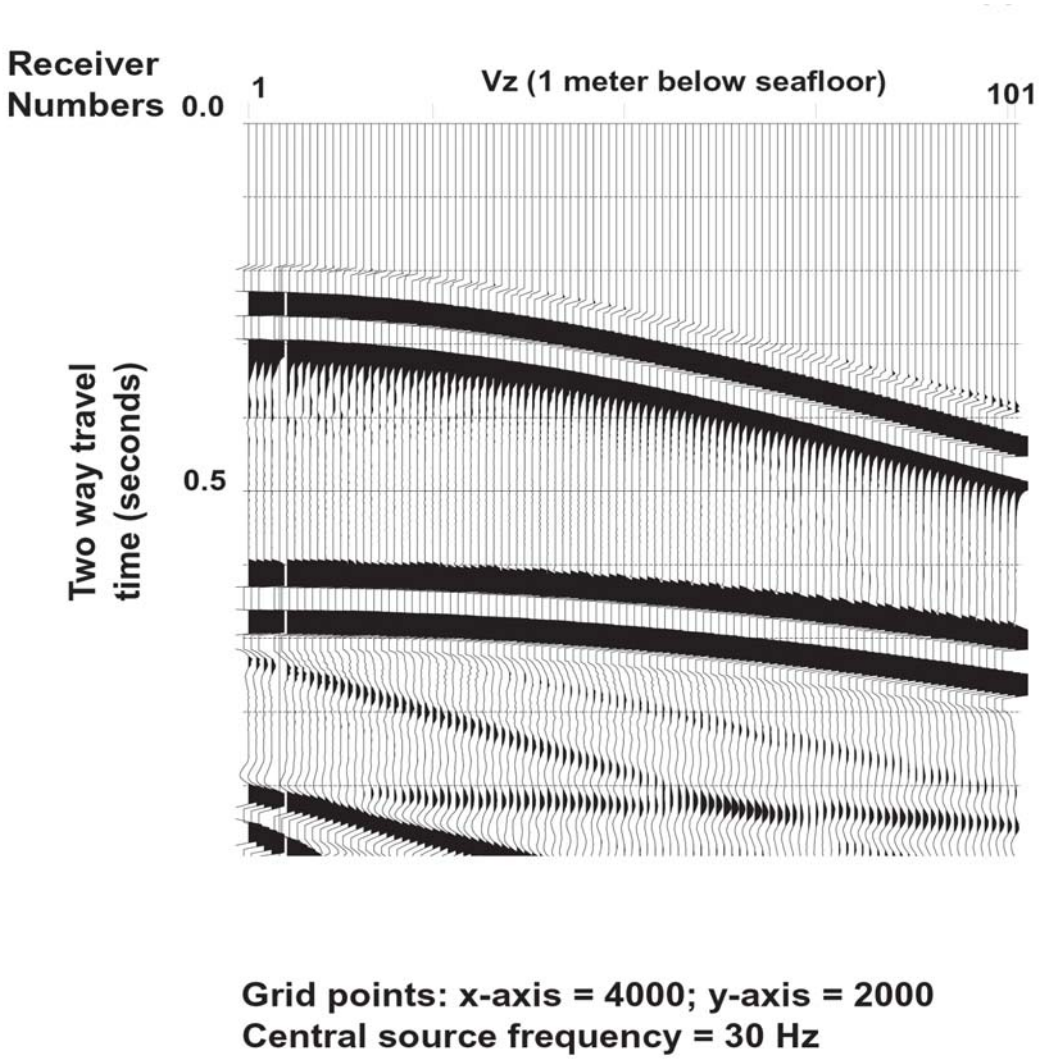

FIG. 36. Shot gather for Vz component of a bad coupled geophone for geological model 2 (flat single layer) with 0.25m discretization spacing. Zero trace at receiver number 5.

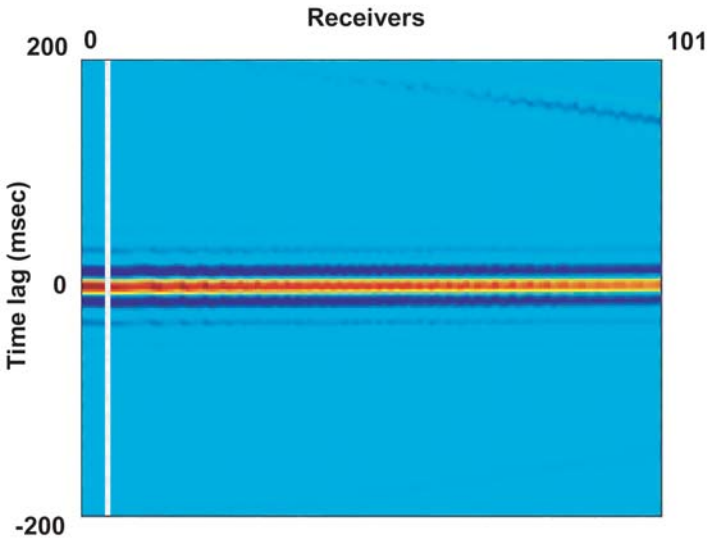

FIG. 37. Normalized cross-correlation between Vz (above seafloor) and Vz (below seafloor) for geological model 2 correspond to zero trace case.

Figure 24 shows very distinctive signature of maximum correlation value being offset in time lag for badly coupled trace. For a dim trace (Figure 34) the maximum correlation value is not offset in time lag. However, a bad trace can be easily identified by a flat correlation value at all time lag for that receiver (Figure 37). Maximum cross-correlation values when compared in conjunction with maximum absolute amplitude values (Figure 22, Figure 32, and Figure 35), they can be used to distinguish between poor coupling, bad and dim trace.

Robustness of cross-correlation

Interestingly, the cross-correlation values for vertical velocity above and below the seafloor show a flat maxima near zero time lag in all the modeling experiments (Figures 38 - 40). Therefore, normalized cross-correlation value is independent of dip

and subsurface geology. As a result normalized cross-correlation between vertical velocities can be a powerful diagnostic tool to identify problem in the OBS surveys rather than the effect of complex subsurface geology and seafloor.

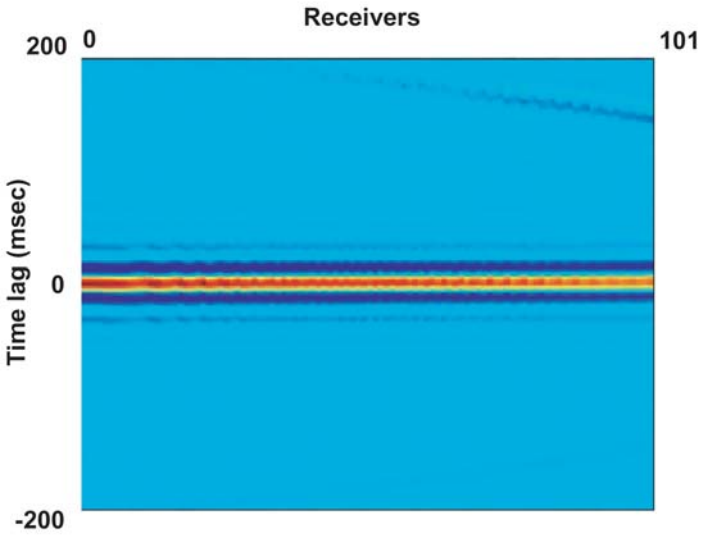

FIG. 38. Normalized cross-correlation between Vz (above seafloor) and Vz (below seafloor) for geological model 1 (flat single layer with 0.25m discretization spacing).

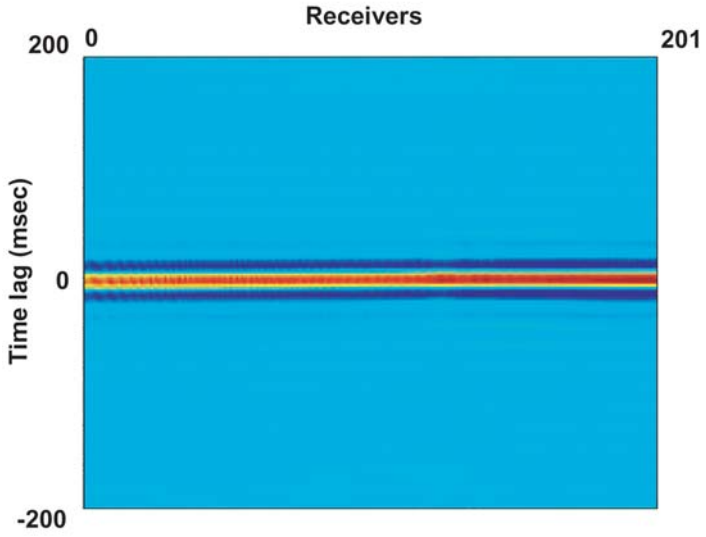

FIG. 39. Normalized cross-correlation between Vz (above seafloor) and Vz (below seafloor) for geological model 3 (single layer with dip 8.5^{o}).

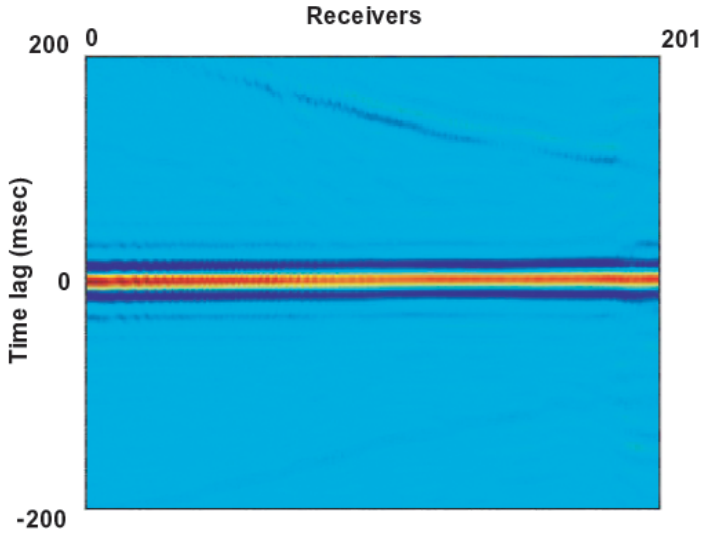

FIG. 40. Normalized cross-correlation between Vz (above seafloor) and Vz (below seafloor) for geological model 5 (complex subsurface geology).

CHAPTER IV

REAL DATA TEST: EUGENE ISLAND 4C DATA

CHALLENGES AHEAD FOR REAL TIME STRATEGY

A major objective for this study was to identify real time diagnostic tools for poor coupling, local orientation in real data. All of our numerical experiments presented above in the text dealt with the investigation of vertical velocity values above and below the seafloor. As we know that it is not possible to directly measure velocity values above the seafloor. Therefore we use reciprocity theorem to convert pressure measurement in vertical source array survey to compute the vertical velocity values above the seafloor. However, real time analysis we investigated a normalized cross-correlation between pressure data from a hydrophone and geophone data (velocity values from below the seafloor). Similar to the normalized cross-correlation values computed for velocity values, one notice correlation is not affected by dip and other heterogeneities only in the near offset case. In far offset the correlation values between pressure and velocity have an added complexity (Figure 41). In spite of the above stated assertion, one can use correlation values between hydrophone and geophone as first order pass in identifying poor coupling cases in a real time OBS experiment.

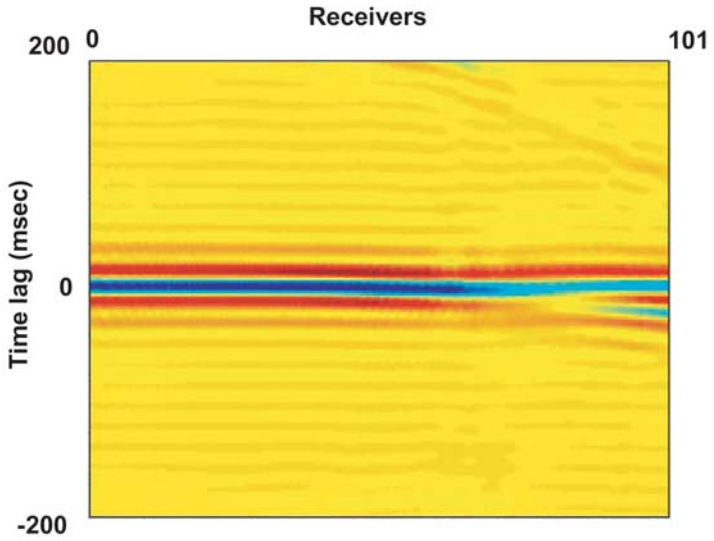

FIG. 41. Normalized cross-correlation between P (above seafloor) and Vz (below seafloor) for geological model 3 (single layer with dip 8.5^{o}).

EUGENE OBS EXAMPLE

To further investigate our idea, I calculated normalized cross-correlation (Figure 42) and total energy ratio (Figure 44) between pressure and vertical velocity data for 4C Eugene Island survey data. Figures 42 and 43 clearly show candidate for poor coupling where there are holes in the correlation maxima near zero time lag. Also figure 44 showed us spike in amplitude value near receiver number 40, 112, and 127. These cases could be due to dim traces in hydrophone (near receiver number 40) and in geophone (near receiver number 127). However, detail investigation needs to be done to identify poor coupling cases in the real data eventough we have identify candidates for them.

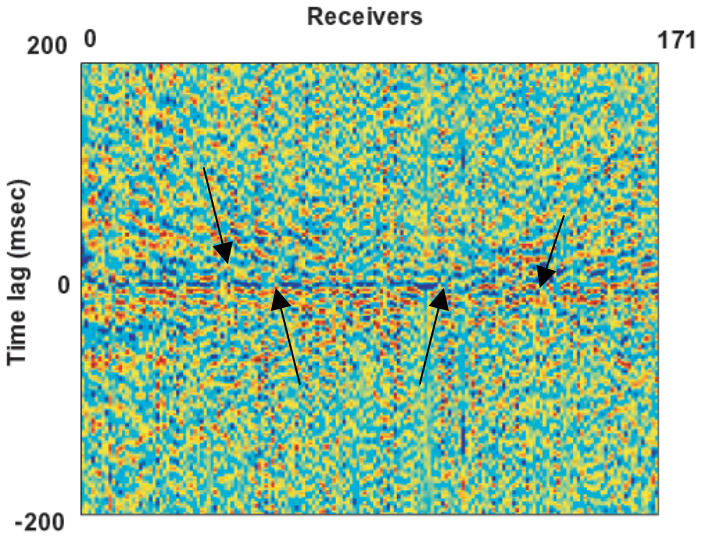

FIG. 42. Normalized cross-correlation between P (above seafloor) and Vz (below seafloor) of Eugene Island seismic data at 5 meters source depth.

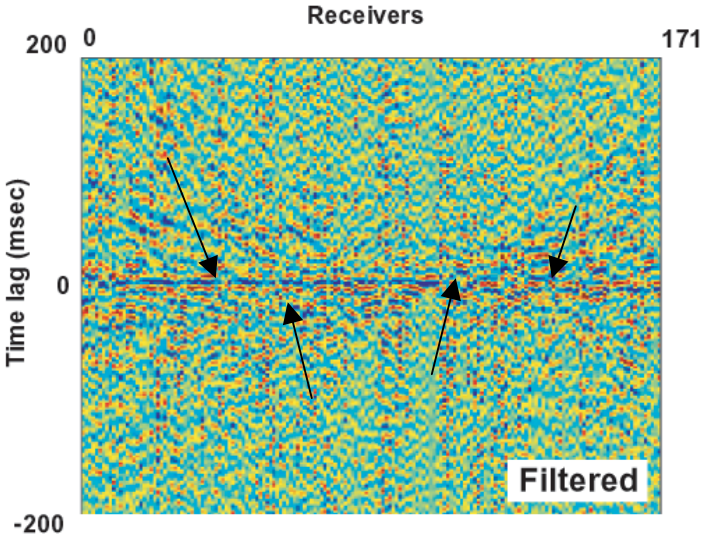

FIG. 43. Normalized cross-correlation between P (above seafloor) and Vz (below seafloor) of Eugene Island seismic data at 5 meters source depth (after frequency data filtered).

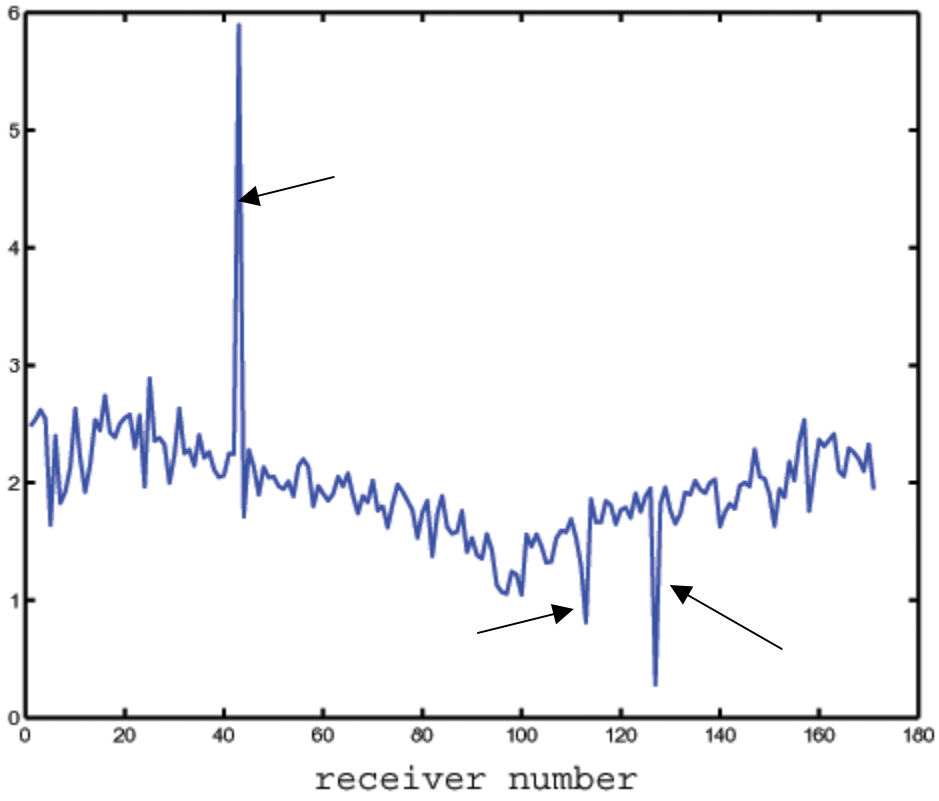

FIG. 44. Total energy ratio between P (above seafloor) and Vz (below seafloor) of Eugene Island data.

CHAPTER V

SUMMARY AND CONCLUSIONS

We have proposed a new way of detecting poor coupling by comparing particle velocity measurements just above and below the seafloor based on continuity conditions. These two measurements must be equal, otherwise we have coupling problem or dipping seafloor effects.

We have developed these two problems using finite-difference synthetic data. For finite-difference, the first test was to simulate the water-solid interface. In fact, due to the finite-difference gridding, we can not put our geophone exactly at the seafloor as in the real experiments. By trial and errors, we established that a grid spacing of 0.25 meters is suitable for simulating water-solid interface. All of subsequence analysis of poor coupling and dipping seafloor effects were carried with 0.25 meters grid spacing.

We have demonstrated that the most suitable grid spacing for modeling seafloor and acoustic-elastic properties is by using 0.25 m grid spacing. Using finite-difference data, we find that a cross-correlation between particle velocity just above and below the seafloor used in conjunction with energy of seismic trace allows us for detecting poor coupling in OBS experiment.

Moreover, amplitude analysis can also be used as a diagnostic tool to identify local dip variations.

From the investigation of the possibility of detecting coupling by comparing pressure (P) in the water with V_z below the water, we found that the normalized cross-correlation correlation is not affected by dip and other heterogenities only in the near offset case. In far offset the correlation values between pressure and velocity have an added complexity. Based on this assertion, one might be able to use correlation values between hydrophone and geophone as first order pass in identifying poor coupling cases in a real time OBS experiment.

To really comment on cases for poor coupling in Eugene data in more detail analysis of the data needs to be done for different shot gathers in a similar way as we did for numerical experiments in this thesis.

REFERENCES

Bayliss, A., Jordan, R.E., LeMesurier, B.J., and Turkel, E., 1986, A fourt-order accurate finite-difference scheme for the computation of elastic waves: Bull. Seis. Soc. Am., **76**, 1115-1132.

Dablain, F.A., 1986, The application of higher-order differencing to the scalar wave equation: Geophysics, **51**, 54-66.

Gaiser, J. E., 1998, Compensating OBC data for variations in geophone coupling: 68th Ann. Internat. Mtg., Soc. Expl. And Geophys., Expanded Abstracts, 1429-1432.

Ikelle, L. T., 1999, Acquisition geometries and seismic data: CASP Project, **7**, 40-64.

Kelly, K. R., Ward, R. W., Treitel S., and Alford R. M., 1976, Synthetic seismograms: A finite-difference approach: Geophysics, **41**, 2-27.

Levander, A. R., 1988, Fourth-order finite-difference P-SV seismograms: Geophysics, **53**, 1425-1436.

Li, X.Y., and Yuan, J., 1999, Geophone orientation and coupling in three-component sea-floor data: a case study: European Association of Geoscientists & Engineers, Geophysical Prospecting, **47**, 995-1013.

Moldoveanu, N., 2000, Vertical source array in marine seismic exploration: 70th Ann. Internat. Mtg., Soc. Expl. Geophys., Expanded Abstracts, 53-56.

Ozdogan, Y., 2001, Seismic data analysis: Processing, inversion, and interpretation of seismic data (2 Vols): Soc. Expl. Geophys.

Virieux, J., 1986, P-SV wave propagation in heterogeneous media: Velocity-stress finite-difference method: Geophysics, **51**, 889-901.

Wilson, R. J., 2002, Potential impacts of vertical cable seismic: Modeling, resolution and multiple attenuation: M. S. Thesis, Texas A&M University, 9-15.

VITA

Fitrix Primantoro Putro was born in 1976 in Jakarta, Indonesia. In 1999, he received his B.S. degree in geophysics from the Institute of Technology of Bandung, Bandung, Indonesia. In 1999 he joined Schlumberger as a geophysicist. His permanent mailing address is: Jl. Pratista Barat VI, No.1, Bandung, West Java, Indonesia. He currently works for China National Offshore Oil Corporation in Jakarta, Indonesia. He is a member of SEG and AAPG.